

The influence of near surface sediment hydrothermalism on the TEX₈₆ tetraether lipid-based proxy and a new correction for ocean bottom lipid overprinting

Jeremy N. Bentley^a, Gregory T. Ventura^a, Clifford C. Walters^b, Stefan M. Sievert^c, Jeffrey S. Seewald^c

^a Department of Geology, Saint Mary's University, Halifax, Nova Scotia B3H 3C3, Canada.

^b Bureau of Economic Geology, University of Texas at Austin, USA.

^c Woods Hole Oceanographic Institution, Woods Hole, USA.

* Corresponding author: Todd.ventura@smu.ca

For submission to *Biogeosciences*

Number of pages: 27

Number of Figures: 6

Number of Tables: 2

Supplementary pages: 6

Key Points

- High *i*GDGTs turnover in shallow sediments is shown to be non-selective and does not impact TEX₈₆ paleoclimate ratios.
- The proxy can be overprinted by sediment sourced lipids when geothermal temperatures rise above ~60–70 °C.
- A diagenetic correction model is presented to remove overprinting artifacts in the TEX₈₆ proxy.

Abstract

The diversity and relative abundances of tetraether lipids produced by archaea and bacteria in soils and sediments are increasingly used to assess environmental change. For instance, the TetraEther indeX of 86 carbon atoms (TEX₈₆), based on archaeal isoprenoidal glycerol dialkyl glycerol tetraether (*i*GDGT) lipids, is frequently applied to reconstruct past sea-surface temperatures (SST). Yet, it is unknown how the ratio fully responds to environmental and/or geochemical variations and if the produced signals are largely the adaptive response by Thaumarchaeota to oceanographic effects associated with climate or seasonal temperature changes in the upper water column. We present the results of a four push-core transect study of surface sediments collected along an environmental gradient at the Cathedral Hill hydrothermal vent system in Guaymas Basin, Gulf of California. The transect crosses a region where advecting hydrothermal fluids reach 155 °C within the upper 21 cm below the seafloor (cmbsf) close to the vent center to near ambient conditions at the vent periphery. The recovered *i*GDGTs closest to the vent center experienced high rates of turnover with up to 94% of the lipid pool being lost within the upper 21 cmbsf. Here, we show that the turnover is non-selective across TEX₈₆ GDGT lipids and does not affect the ratio independently. However, as evident by TEX₈₆ ratios being highly correlated to the Cathedral Hill vent sediment porewater temperatures ($R^2 = 0.84$), the ratio can be strongly impacted by the combination of severe lipid loss coupled with the addition of *in situ* *i*GDGT production from archaeal communities living in the vent sediments. The resulting overprint produces absolute temperature offsets of up to 4 °C based on the TEX₈₆^H-calibration relative to modern climate records of the region. The overprint is also striking given the flux of *i*GDGTs from the upper water column is estimated to be ~93% of the combined intact polar lipid (IPL) and core GDGT lipid pool initially deposited on the seafloor. A model to correct the overprint signal using IPLs is therefore presented that can similarly be

applied to all near-surface marine sediment systems where calibration models or climate reconstructions are made based on the TEX₈₆ measure.

1. Introduction

Archaeal and bacterial tetraether cellular membrane lipids represent a group of common and structurally diverse compounds frequently used to track the presence of living and dead microorganisms as well as geochemical and physical conditions within present-day and paleoenvironments (e.g., Schouten et al., 2002, 2004; 2013; Hopmans et al., 2004; Weijers et al., 2007, 2014; Hollis et al., 2012; O'Brien, et al., 2017; Stuart et al., 2017). In this regard, the proportional abundances of these lipids form various prominent proxies for assessing environmental change through time. For example, TEX₈₆ (TetraEther indeX with 86 carbon atoms; Schouten et al., 2002) is a widely used archaeal lipid-based paleotemperature proxy for marine environments. The ratio measures variations in the number of cyclopentyl rings for a select group of archaeal core lipids (CLs) (Supplementary Figure S1) following the assumption that biphytanyl cyclization is an organismal response to changing sea surface temperatures (SSTs). The proxy is therefore used in many regions around the world with TEX₈₆ values typically ranging from 0.2–0.9 in marine settings (e.g. Huguet et al., 2006; Kim et al., 2008; McClymont et al., 2012; Tierney, 2014). The utility of TEX₈₆ rests on the premise that *i*GDGTs found in ocean bottom sediments are almost exclusively produced by marine planktonic archaea that inhabit the epipelagic zone (Wakeham et al., 2003; Tierney, 2014; Besseling et al., 2019, 2020). Lipids are therefore required to be efficiently and continually transported from the upper water column to the underlying ocean floor to produce a fossil chemostratigraphic record of microbial response to changing SST conditions with time (Wuchter et al., 2005).

Since its introduction, the reliability of TEX₈₆ to accurately track paleoclimate variations has been questioned. TEX₈₆-based SST estimates have been observed to substantially deviate from other temperature proxies (e.g. Huguet et al., 2006; Rommerskirchen et al., 2011; Seki et al., 2012). For example, over the past decade, considerable effort has been made to reconstruct the early Paleogene greenhouse climate system. However, TEX₈₆ appears to significantly over-estimate reconstructed SSTs (Hollis et al., 2012) relative to other proxies such as Mg/Ca, or clumped isotopic compositions of foraminiferal calcite, as well as various climate models based on partial pressure of carbon dioxide ($p\text{CO}_2$) predictions (Lunt et al., 2012; Naafs et al., 2018). For late Neogene climate reconstructions, TEX₈₆ has been shown to underestimate warming trends relative to the $U_{37}^{K'}$ alkenone-index (Brassell et al., 1986) derived temperatures (Lawrence et al., 2020). The apparent SST offsets have been attributed to how the proxy's associated lipids change in relation to their environment and if these changes are regulated by internal adaptations within the archaeon or by an overarching community succession. In this regard, the debate surrounding these discrepancies largely centers on establishing responses to seasonal biases (e.g. Herford et al., 2006; Wuchter et al., 2006; Huguet et al., 2011); the development of adequate calibration methods (e.g. Kim et al., 2010; Pearson et al., 2013; Tierney et al. 2014); identifying lipid sourcing effects – including subsurface sediments origins for those used with the calculation of TEX₈₆ (e.g. Lipp and Hinrichs, 2009); as well as physical, chemical, and ecological controls for archaeon *i*GDGTs cyclization (e.g. Elling et al., 2015; Qin et al., 2015; Hurley et al., 2016).

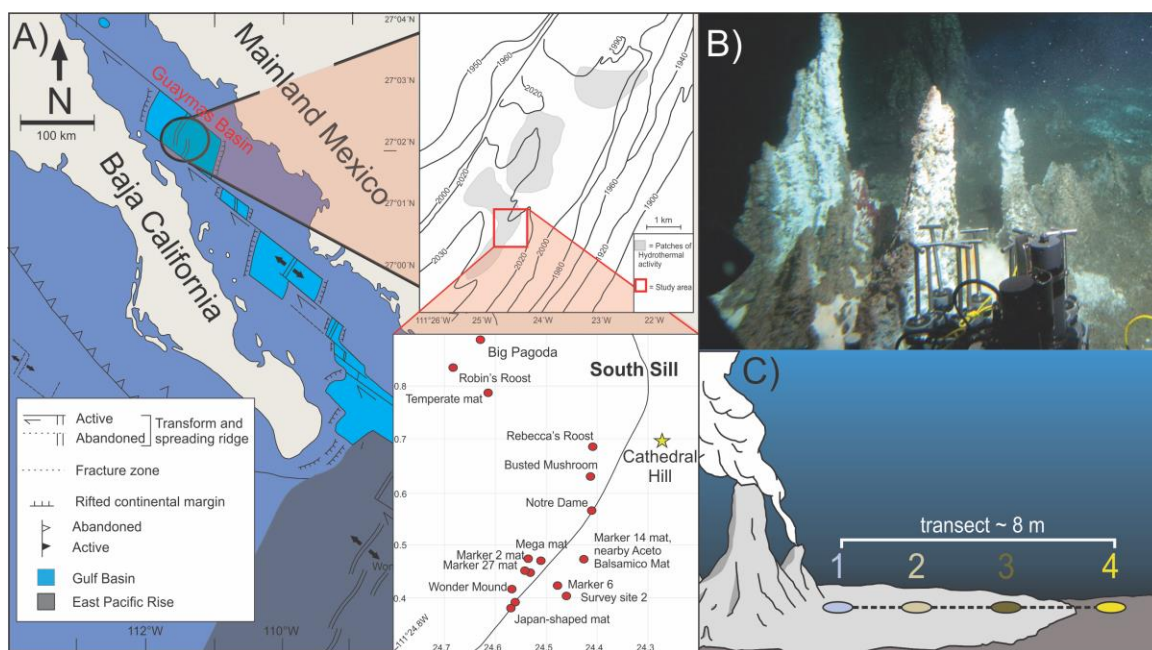
For non-thermal influences, the primary concern is what archaeal taxa produce *i*GDGTs and where they are sourced. To this end, most TEX₈₆ lipids are thought to be produced by Marine Group I (MGI) planktonic Thaumarchaeota (Brochier-Armanet et al., 2008), which are most abundant below the photic and epipelagic zone (e.g., Karner et al., 2001). Within this context, many regions of the ocean floor may become highly impacted by colder, deeper water column inputs (e.g. Karner et al., 2001; Huguet et al., 2007; Lopes dos Santos et al., 2010; Kim et al., 2012a,b; Pearson et al., 2013; Kim et al., 2015; Ho & Laepple, 2016; Hurley et al., 2016; Lui et al., 2018; Sinninghe Damsté et al., 2018). Other non-thermogenic driving forces impacting the production, cyclization, and relative abundance of TEX₈₆-based lipids include organismal selectivity to specific growth phases and growth rates (Elling et al., 2014; Hurley et al., 2016); redox conditions (Qin et al., 2015); and the incorporation of *i*GDGT from archaeal communities living in the ocean floor sediments. With respect to the latter, Lipp and Hinrichs (2009) demonstrated that the production of intact polar lipid GDGTs (IPL-GDGTs) by ocean floor sediment microbial communities collected in the Peru Margin were distinctly different from upper water column sourced CLs and that the conversion of this living pool to fossil lipids would shift TEX₈₆ ratios to higher values. However, the overall impact may not be substantial as Umoh et al.

107 (2020) found little effect to the TEX₈₆ paleoclimate ratio when examining surface sediments near
108 hydrothermal vent sites on the Southeast Indian Ridge in the southern Indian Ocean. Lengger et al. (2012,
109 2014) also reported no significant deviation between the TEX₈₆ values in sediment cores collected near the
110 oxygen minimum zone from that of the overlying water column in the Arabian Sea with near linear
111 degradation rates of both IPLs and CLs. All together, the *i*GDGT abundances recorded in a TEX₈₆ sediment
112 value may ultimately constitutes a multi-variable datapoint – mixing lipid components that are themselves
113 responses to: temperature, organismal substrate and metabolism dynamics, biozone niche partitions spanning
114 from the ocean surface to the shallow sediment archaeal community, which ultimately become further
115 attenuated by depositional and diagenetic processes.

116
117 While not an ideal location to create SST reconstructions, hydrothermal vents of sedimented ocean basins do
118 represent an anomalous endmember to the vast expanse of ambient ocean floor sediment where paleoclimate
119 reconstructions are commonly produced. The sedimented vent systems of Guaymas Basin, Gulf of California
120 (Figure 1) is one such site. The basin experiences high sedimentation rates ranging from 0.4–0.2 cm yr⁻¹
121 (Curry et al., 1979; Gieskes et al., 1988) due in part to the high productivity of the upper water column. The
122 ocean floor hydrothermally impacted surface sediments are also a location of active and diverse microbial
123 communities with vents that are often covered by Beggiatoa dominated microbial mats (e.g. McKay et al.,
124 2012; Meyer et al., 2013; Teske et al., 2016). These sites should in principle, enable a high-resolution archaeal
125 lipid stratigraphic record that provides optimal conditions for studying potential shallow diagenetic and
126 subseafloor interferences to common archaeal lipid-based environmental proxies. The region further offers
127 an ideal setting to compare TEX₈₆ proxy responses to *in situ* lipid production from thermophilic sedimentary
128 archaea that differ from the pelagic background communities (e.g. Schouten et al., 2003). Recently, Bentley
129 et al. (2022) produced a survey of the source and diagenetic and catagenetic alteration of archaeal lipids from
130 the Cathedral Hill hydrothermal vent complex (Figure 1) in the Guaymas Basin, Gulf of California. Within
131 the investigation, it was observed that most *i*GDGTs are sourced from the overlying water column. Building
132 on the results of Schouten et al. (2003), it was observed that these lipids can become heavily turned over in
133 the hotter portions of the vent site where they rarely survive long enough to become cracked into hydrocarbon
134 biomarkers such as biphytanes and derivatives of biphytanes. For this study, we further examine the *i*GDGT
135 lipid distributions in these near-surface ocean floor sediments to determine if paleoclimate proxy signals can
136 be impacted by the presence of subsurface archaeal populations. The distribution of *i*GDGTs and their
137 corresponding environmental proxy signals were measured within the sediments along a transect at the
138 complex. In this regard, this site offers the unique opportunity to evaluate the response of TEX₈₆ and other
139 tetraether-lipid proxies within a microbially diverse sedimentary environment that is exposed to high
140 temperature vent fluids.

141
142

143



144

145 **FIGURE 1** A) Location map of Guaymas Basin and the Southern Sill (red outlined box) in the Gulf of
 146 California. Cathedral Hill is marked with a yellow star. B) Photo of Cathedral Hill taken via *Alvin*. C)
 147 Schematic of the push core transect with a color-coding that is consistent for all plots throughout this paper.
 148 Maps modified from Teske et al. (2016), Dalzell et al. (2021), and Bentley et al. (2022).

149

150 2. Material and methods

151 2.1. Study location and sampling

152 Four sediment push cores were collected using HOV *Alvin* (Dive 4462; 10/22/08) at the Cathedral Hill
 153 hydrothermal vent site, located at a water depth of 1996 m in the Southern Trough of Guaymas Basin, Gulf
 154 of California (27°0.629' N, 111°24.265' W) (Figure 1). The push cores, labeled 1 to 4, were taken along a
 155 transect with ~ 2 m spacing extending outwards from microbial mat-covered sediments near the sulfide
 156 chimney complex to just outside of the microbial mat area in ambient seafloor sediment. Thermal-probe
 157 measurements were sequentially taken beside each core (Table 1). Once the push cores were brought to the
 158 surface, the sediments were subsampled into 2–3 cm-thick depth intervals, transferred to combusted glass
 159 vials, and immediately stored at -40 °C (onboard the ship) before being shipped under dry ice to the laboratory
 160 and later freeze-dried and stored at -80 °C.

161

162

163

164

165

166

167

168

169

170

171

172

173 **Table 1.** Cathedral Hill sample push core, sediment, geochemical, and lipid proxy data.
174

Core ^a	Depth interval (cmbf)	Alvin dive # and core ID	Description/lithology ^b	Pore water temperature (°C) [*]	Interpolated Pore water temperature (°C) [*]	Sediment weight (g) ⁺	TLE (mg g sed ⁻¹) ⁺	Sum of IPL iGDGT (μg g ⁻¹) [†]	Sum of iGDGT (μg g ⁻¹) [‡]
1	0-2	GB4462-5	Black mud with microbial mat filaments	19	19	1.97	11.5	16.7	503.1
1	2-4	GB4462-5	Brownish-green diatomaceous mud	-	67	2.04	7.65	14.6	461.7
1	4-6	GB4462-5	Brownish-green diatomaceous mud	85	85	2.03	9.37	6.0	203.3
1	6-8	GB4462-5	Brownish-green diatomaceous mud	-	105	1.99	2.09	4.3	148.6
1	8-10	GB4462-5	Brownish-green diatomaceous mud	-	117	2.01	4.38	3.2	59.0
1	10-12	GB4462-5	Grayish-green mud	121, 124	125	2.01	1.97	1.7	48.8
1	12-15	GB4462-5	Brownish-green consolidated mud with clay shards	-	135	1.98	1.99	1.4	78.7
1	15-18	GB4462-5	Brownish-green consolidated clay	142	145	1.96	1.69	0.0	42.6
1	18-21	GB4462-5	Brownish-green consolidated clay	153	153	1.98	1.72	0.0	38.4
2	0-2	GB4462-6	Black mud with microbial mat filaments	9, 13	11	2.02	8.48	17.8	591.0
2	2-4	GB4462-6	Black mud with microbial mat filaments	-	22	1.97	8.65	7.5	266.3
2	4-6	GB4462-6	Brownish-green diatomaceous mud	20	20	1.95	2.51	2.5	87.4
2	6-8	GB4462-6	Brownish-green diatomaceous mud	-	47	1.95	3.38	3.4	69.7
2	8-10	GB4462-6	Brownish-green diatomaceous mud	-	60	1.95	1.48	2.0	48.4
2	10-12	GB4462-6	Brownish-green diatomaceous mud	69, 77	73	1.94	4.19	2.0	52.1
2	12-15	GB4462-6	Brownish-green diatomaceous mud	-	87	2.02	1.69	1.0	44.2
2	15-18	GB4462-6	Brownish-green diatomaceous mud	118	105	1.95	2.01	0.0	22.3
2	18-21	GB4462-6	Brownish-green diatomaceous mud	109	125	1.94	1.38	0.0	31.2
3	0-2	GB4462-3	Black mud with microbial mat filaments	3.2	3.2	1.96	7.31	15.3	511.3
3	2-4	GB4462-3	Brownish-green diatomaceous mud	-	8	1.96	3.91	8.3	308.9
3	4-6	GB4462-3	Brownish-green diatomaceous mud	15	15	2.00	2.86	7.0	283.5
3	6-8	GB4462-3	Brownish-green diatomaceous mud	-	26	2.02	5.00	7.5	275.3
3	8-10	GB4462-3	Brownish-green diatomaceous mud	34	34	1.97	2.02	5.7	251.1
3	10-12	GB4462-3	Brownish-green diatomaceous mud	-	43	2.01	1.86	5.8	227.7
3	12-15	GB4462-3	Brownish-green diatomaceous mud	-	54	1.94	1.78	6.5	184.6
3	15-18	GB4462-3	Brownish-green diatomaceous mud	61	66	2.01	1.43	12.3	473.1
3	18-21	GB4462-3	Brownish-green diatomaceous mud	83	80	1.96	1.98	5.2	182.3
4	0-2	GB4462-8	Black mud	0	0	1.93	3.44	16.7	485.4
4	2-4	GB4462-8	Brownish-green diatomaceous mud	1.5	8	2.01	3.17	14.6	417.8
4	4-6	GB4462-8	Brownish-green diatomaceous mud	16	16	1.95	4.00	6.0	480.6
4	6-8	GB4462-8	Brownish-green diatomaceous mud	-	18	2.02	4.19	4.3	359.7
4	8-10	GB4462-8	Brownish-green diatomaceous mud	-	21	2.02	4.76	3.2	153.5
4	10-12	GB4462-8	Brownish-green diatomaceous mud	-	23	1.95	4.84	1.7	459.5
4	12-15	GB4462-8	Brownish-green diatomaceous mud	-	25	1.95	5.74	1.4	515.2
4	15-18	GB4462-8	Sample lost during collection	-	-	-	-	0.0	503.1
4	18-21	GB4462-8	Sample lost during collection	29	-	-	-	0.0	461.7

175
176
177
178
179
180
181
182
183
184
185
186
187
188
189
190
191
192
193
194
195
196

197 **Table 1.** Cathedral Hill sample push core, sediment, geochemical, and lipid proxy data (continued).
198

Core ^a	Depth interval (cmbsf)	Alvin dive # and core ID	SUM of TEX ₈₆ cGDGT ^c (µg g ⁻¹)	TEX ₈₆ cGDGT ^c	TEX ₈₆ ^H cGDGT ^d	TEX ₈₆ ^H Reconstructed SSTs (Kim et al., 2010) ^e	RI ^f	MI ^g	TEX ₈₆ IPLGDGT ^c
1	0-2	GB4462-5	110.7	0.56	-0.25	21.2	2.44	0.34	0.58
1	2-4	GB4462-5	117.1	0.58	-0.23	22.6	2.45	0.38	0.58
1	4-6	GB4462-5	47.7	0.58	-0.24	22.3	2.48	0.36	0.55
1	6-8	GB4462-5	33.0	0.58	-0.24	22.2	2.55	0.35	0.57
1	8-10	GB4462-5	13.0	0.59	-0.23	22.9	2.60	0.34	0.72
1	10-12	GB4462-5	10.1	0.57	-0.25	21.8	2.63	0.31	0.70
1	12-15	GB4462-5	17.8	0.61	-0.22	23.8	2.65	0.37	0.69
1	15-18	GB4462-5	9.8	0.61	-0.22	23.9	2.66	0.36	-
1	18-21	GB4462-5	9.3	0.63	-0.20	24.9	2.66	0.38	-
2	0-2	GB4462-6	128.5	0.55	-0.26	20.6	2.52	0.32	0.46
2	2-4	GB4462-6	58.2	0.54	-0.27	20.4	2.52	0.32	0.58
2	4-6	GB4462-6	19.2	0.54	-0.27	20.4	2.53	0.33	0.60
2	6-8	GB4462-6	13.4	0.56	-0.25	21.5	2.68	0.29	0.71
2	8-10	GB4462-6	9.3	0.58	-0.25	21.7	2.70	0.29	0.70
2	10-12	GB4462-6	10.1	0.57	-0.24	21.9	2.71	0.28	0.68
2	12-15	GB4462-6	8.5	0.57	-0.24	21.9	2.73	0.28	0.73
2	15-18	GB4462-6	4.5	0.58	-0.23	22.6	2.68	0.31	-
2	18-21	GB4462-6	6.0	0.59	-0.23	22.8	2.74	0.28	-
3	0-2	GB4462-3	127.0	0.54	-0.27	20.2	2.41	0.37	0.53
3	2-4	GB4462-3	57.7	0.53	-0.27	19.8	2.62	0.27	0.49
3	4-6	GB4462-3	60.0	0.53	-0.27	19.9	2.53	0.31	0.56
3	6-8	GB4462-3	59.8	0.54	-0.27	20.3	2.50	0.33	0.54
3	8-10	GB4462-3	53.0	0.53	-0.27	19.9	2.54	0.31	0.61
3	10-12	GB4462-3	42.1	0.54	-0.27	20.3	2.64	0.27	0.74
3	12-15	GB4462-3	39.2	0.56	-0.25	21.5	2.56	0.30	0.69
3	15-18	GB4462-3	86.8	0.55	-0.26	20.9	2.77	0.26	0.74
3	18-21	GB4462-3	36.4	0.57	-0.25	21.6	2.68	0.29	0.66
4	0-2	GB4462-8	112.9	0.54	-0.27	20.4	2.43	0.35	0.54
4	2-4	GB4462-8	85.3	0.53	-0.27	20.0	2.59	0.30	0.37
4	4-6	GB4462-8	102.7	0.54	-0.27	20.2	2.55	0.31	0.43
4	6-8	GB4462-8	70.8	0.52	-0.28	19.3	2.55	0.29	0.45
4	8-10	GB4462-8	26.6	0.53	-0.27	19.9	2.69	0.26	-
4	10-12	GB4462-8	91.0	0.53	-0.27	19.8	2.54	0.30	-
4	12-15	GB4462-8	73.7	0.53	-0.28	19.7	2.90	0.20	-
4	15-18	GB4462-8	110.7	-	-	-	-	-	-
4	18-21	GB4462-8	117.1	-	-	-	-	-	-

199 * Also reported in Bentley et al. (2022).

200 † Sum of GDGT-1, -2, -3, -4, -5' (Table S1).

201 ‡ Sum of all detected 1G- and 2G-GDGTs (Table S3).

202 ^a Collected core numbers are relabelled in the sample name to reflect a relative transect position (1-4).

203 ^b Sediment lithology based on freeze-dried sediments.

204 ^c TEX₈₆ = (GDGT-2 + GDGT-3 + GDGT-5')/(GDGT-1 + GDGT-2 + GDGT-3 + GDGT-5'), (Schouten et al., 2002) applied to both core GDGTs and 1-glycosyl-GDGTs (also referred to as *M*TEX₈₆ in section 3.4).

205 ^d TEX₈₆^H = log ((GDGT-2 + GDGT-3 + GDGT-5')/(GDGT-1 + GDGT-2 + GDGT-3 + GDGT-5')), for
206 sediments outside low latitudes (Kim et al., 2010).

207 ^e Following the mean annual sea surface calibration of 0 m water depth (SST = 68.4 × TEX₈₆^H + 38.6) of
208 Kim et al. (2010).

209 ^f Ring index (RI) = 0×(GDGT-0) + 1×(GDGT-1) + 2×(GDGT-2) + 3×(GDGT-3) + 4×(GDGT-4) +
210 5×(GDGT-5)/ ΣGDGTs, adapted from Pearson et al. (2004) and promoted by Zeng et al. (2016).

211 ^g Methane index (MI) = (GDGT-1 + GDGT-2 + GDGT-3)/(GDGT-1 + GDGT-2 + GDGT-3 + GDGT-5 +
212 GDGT-5') by Zhang et al. (2011).

213

214

215

216

217

218

219

2.2. Lipid extraction

Lipid extractions followed a modified Bligh and Dyer protocol laid out in Bentley et al. (2022) and following Sturt et al. (2004). A subsample of freeze-dried sediment was added to a Teflon[®] centrifuge tube followed by the addition of 6 ml of mix A solvent solution comprising of 2:1:0.8 v/v/v methanol (MeOH), dichloromethane (DCM), and phosphate buffer (5.5 g L⁻¹ Na₂HPO₄; Avantor Performance Materials, LLC. adjusted to pH of 7.4 with HCl; Anachemia Co.). The solvent sediment mixture was further spiked with 1-alkyl-2-acetoxy-*sn*-glycero-3-phosphocholine (PAF) recovery standard purchased from Avanti Polar Lipids, Inc. The slurry was sonicated for 5 min then centrifuged for 5 min at 1250 rpm. The resulting supernatant was added to a separatory funnel. This procedure was performed twice before being joined by two replicate extractions using mix B, a 2:1:0.8; v/v/v solution of MeOH, DCM, and trichloroacetic acid buffer (50 g L⁻¹ C₂HCl₃O₂; Avantor Performance Materials, LLC. of pH 2) and a final two replicate extractions using mix C, a 5:1 v/v solution of MeOH and DCM. Once complete, the combined A, B, and C. For each step, the organic fraction was collected in a beaker, and the combination of mix A, B, and C were subjected to 10 ml of DCM and H₂O (MilliQ) to achieve separation. The organic phase was drawn off and the water was extracted using 3 DCM washes, drawing off the organic phase after each wash. The organic phase was back-extracted with H₂O to ensure purity. The resulting organic phase was then evaporated to dryness at 60 °C under dry nitrogen. The resulting total lipid extract (TLE) was transferred to pre-weighed autosampler vials using DCM:MeOH 1:1 v/v, spiked with 1, 2-diheneicosanoyl-*sn*-glycero-3-phosphocholine (C₂₁-PC; Avanti Polar Lipids, Inc.) and stored at -20 °C.

2.3. High performance liquid chromatography – mass spectrometry (HPLC-MS)

Mass spectrometric analyses were performed on an Agilent Technologies 1260 Infinity II HPLC coupled to an Agilent Technologies 6530 quadrupole time-of-flight mass spectrometer (qToF-MS) operated in positive mode. Chromatographic separation used a reverse-phase method outlined by Zhu et al. (2013). The HPLC was fitted with an Agilent Technologies ZORBAX RRHD Eclipse Plus C₁₈ (2.1 mm × 150 mm × 1.8 μm) reverse phase column and guard column maintained at 45 °C. The sample injection solvent was methanol. An aliquot of each sample representing 1% of the TLE was analyzed. A 0.25 mL min⁻¹ flow rate was established with mobile phase A consisting of methanol/formic acid/ammonium hydroxide (100:0.04:0.10 v/v/v) held at 100% for 10 min, thereafter mixed following a linear gradient with mobile phase B (propan-2-ol/formic acid/ammonium hydroxide (100:0.04:0.10 v/v/v) to 24%, 65%, and 70% over 5-, 75-, and 15-min intervals, respectively. Each sample run was finished by re-equilibrating the system with 100% mobile phase A for 15 min. The effluent was ionized by an electrospray ionization source with a gas temperature of 300 °C, a 3 L min⁻¹ drying gas flow, and a 5.33 μA source current. The mass spectrometer was set to a 100–3000 *m/z* scan range in positive mode in an untargeted method with 10 ppb resolution to simultaneously resolve both archaeal IPLs and CLs.

Analyte identification was achieved by accurate mass resolution, mass spectral analysis using Agilent Technology's MassHunter software, and comparison of fragmentation patterns with the literature (e.g., Knappy et al., 2009; Liu et al., 2010; Yoshinaga et al., 2011 – see Bentley et al., 2022 for further details). Mass fragments consistent with the loss of a biphytane (*m/z* 743.7) were screened for all archaeal lipids. Quantification was achieved by summing the integration peak areas of [M+H]⁺, [M+NH₄]⁺, and [M+Na]⁺ adducts for the respective IPLs and CLs of interest. Concentration values were obtained relative to the internal C₂₁-PC standard and reported in μg g⁻¹ dry sediment weight. Response factors were determined by a series of injections of a standard solution containing: PAF, C₂₁-PC, 1,2-diacyl-3-O-(α-D-galactosyl)-β-D-galactosyl-*sn*-glycerol (DGDG), 1,2-diacyl-3-O-β-D-galactosyl-*sn*-glycerol (MGDG), 1,2-di-O-phytan-3-yl-*sn*-glycerol (archaeol), 1',3'-bis[1,2-dimyristoyl-*sn*-glycero-3-phospho]-glycerol (14:0 Cardiolipin) from Avanti Polar Lipids, Inc., USA, and 2,2'-di-O-decyl-3,3'-di-O-(1'',ω''-eicosanyl)-1,1'-di-(rac-glycerol) (C₄₆-GTGT) from Pandion Laboratories, LLC in amounts ranging from 100 pg to 30 ng. Response factors were calculated relative to the C₂₁-PC, and the appropriate correction factor was then applied to the lipid class of interest.

A series of samples were re-run to identify or confirm deviations in the data set. The variations between the concentrations of GDGTs in the re-run and the initial runs yielded a maximum difference of ~ ± 4 μg g⁻¹ per

GDGT compound, providing confidence in the initial results and confirming the presence of two outliers in the data set (Bentley et al., 2022). These outliers are Core 4 at 8–10 cm, with abnormally low concentrations of all compounds that are likely ion suppression from a sample heavily impregnated with oil, and Core 3 at 15–18 cm, which contains relatively high lipid concentrations that are yet to be explained.

3. Results and Discussion

3.1. Archaeal lipid diversity and turnover

The Cathedral Hill transect sediments have *i*GDGTs containing 0–4 cyclopentyl (GDGT 0–4) as well as crenarchaeol (Cren) and the isomer of crenarchaeol (Cren') that contains five rings (four cyclopentyl and one cyclohexyl moiety) (Table S1). Branched GDGTs (*br*GDGTs) including Ia-c, IIa-c, and IIIa were found to have discontinuous and/or low absolute abundances, with some compound classes not being detected (i.e. *br*GDGT-IIIb; Table S2). The *br*GDGTs are therefore not further examined in this study. For cores 1 to 3 the concentrations of nearly all *i*GDGT compounds systematically decrease with depth (Figure 2). Bentley et al. (2022) established the sedimentation of archaeal lipids from the upper water column as being uniform both in terms of spatial loading across the length of the transect as well as over an inferred 52.5–105 yrs of sedimentation as penetrated by the length of the push core (based on sedimentation rates). From this, it is estimated that $\sim 70.6 \pm 23.5 \mu\text{g } i\text{GDGTs g}^{-1} \text{ sed yr}^{-1}$ is being deposited on the seafloor from the overlying water column. However, for cores closest to the vent site, lipid abundances exhibited a much sharper decrease with depth, which Bentley et al. (2022) attribute to the turnover of archaeal lipids coupled to, but not directly caused by, hydrothermalism. For cores 1 and 2, losses reach as high as 94% within the upper 21 cmbsf (cm below seafloor). The lipid loss is less severe for core 3 at $\sim 60\%$. For the ambient core 4, *i*GDGTs have similar down core stratigraphic trends with a near-consistent average of $400 \mu\text{g g}^{-1}$ sediment concentration and no systematic loss of lipids.

Due to the high temperature conditions of the vent fluids at Cathedral Hill, the identified archaeal *i*GDGT-based IPLs within the sediments most likely represent the composition of cellular membrane material from archaeal communities living in the sediments. These lipids have exclusively monoglycosyl (1G) or diglycosyl (2G) head groups linked to a 2,3-sn-glycerol. Within the pyrolytic environment, the transformation of IPL *i*GDGTs could hypothetically add to the core *i*GDGT lipid pool. Similar to CLs, the 1G-GDGTs contain 0–4 cyclopentyl moieties and include Cren and Cren'. Surface concentrations of these lipids are $\sim 15 \mu\text{g g}^{-1} \text{ sed.}$ in cores 1 to 3 (residing within the microbial mat) and $11 \mu\text{g g}^{-1} \text{ sed.}$ for core 4 (Table S2). Also similar to the CLs, the archaeal IPL concentrations decrease down core and are closely coupled to increasing porewater temperatures (Table S2). For cores 1 and 2, the maximum depths for detectable 1G-GDGTs are 15–18 and 12–15 cmbsf, corresponding to vent porewater temperatures of 145 and 87 °C, respectively. In core 3, 1G-GDGTs persist down core with a consistent lipid depletion that reaches its lowest concentration of $5.2 \mu\text{g g}^{-1} \text{ sed.}$ in the bottom of the core at 18–21 cmbsf sediment depth where porewater temperatures rise to 80 °C. In core 4, which is most similar to the ambient ocean bottom conditions and falls outside of the area covered by the microbial mat, the lipid concentrations average is $\sim 8 \mu\text{g g}^{-1} \text{ sed.}$ across the depth of the core. The 2G-GDGTs have 0 to 2 cyclopentyl rings that for cores 1 and 2 are restricted to the upper 4 to 6 cmbsf. These lipids are not further investigated in this study as 2G-GDGTs are of limited abundance (max summed concentrations $< 2 \mu\text{g g}^{-1} \text{ sed.}$) and their structural diversities negligibly affect isoprenoid-based proxies.

Lipid-based proxies for the calibration or reconstruction of paleoclimate records such as TEX₈₆ are based on environmentally scaled contributions of select GDGT compounds. These proxies could be negatively impacted should other ocean floor sediment systems experience high rates of lipid turnover (Lengger et al., 2014). To evaluate whether down-core depletions of lipid concentrations impacted tetraether-based proxies, the concentrations of the highly abundant GDGT-0 was plotted relative to the TEX₈₆ ratio lipids (*i*GDGT-1, -2, -3, and Cren') (Figure 3A). For figure 3A, straight lines in the logarithmic plot indicate near-equal depletion rates between the paired x- and y-axis lipid classes. Similarly, parallel slopes for the various lipid pairs also indicates near-equal depletion rates, with vertical offsets between pairs marking different initial starting abundances of the compared lipid. In this regard, *i*GDGT-0, -1, -2, and Cren' have undergone the same rate of turnover. However, the depletion rate of *i*GDGT-3's is lower than that of other lipid classes for cores 1 and

2. Although, this may represent a distinct resilience to turnover, we suggest it instead results from overprinting by the subsurface hyperthermophilic archaeal community (see below).

To better track changes across each core, the degradation rate constants (k') of TEX₈₆ lipid classes were calculated for each push core (Figure S2; Table S3) using a first-order kinetic model:

$$C_t = C_i \cdot e^{-k't} \quad (1)$$

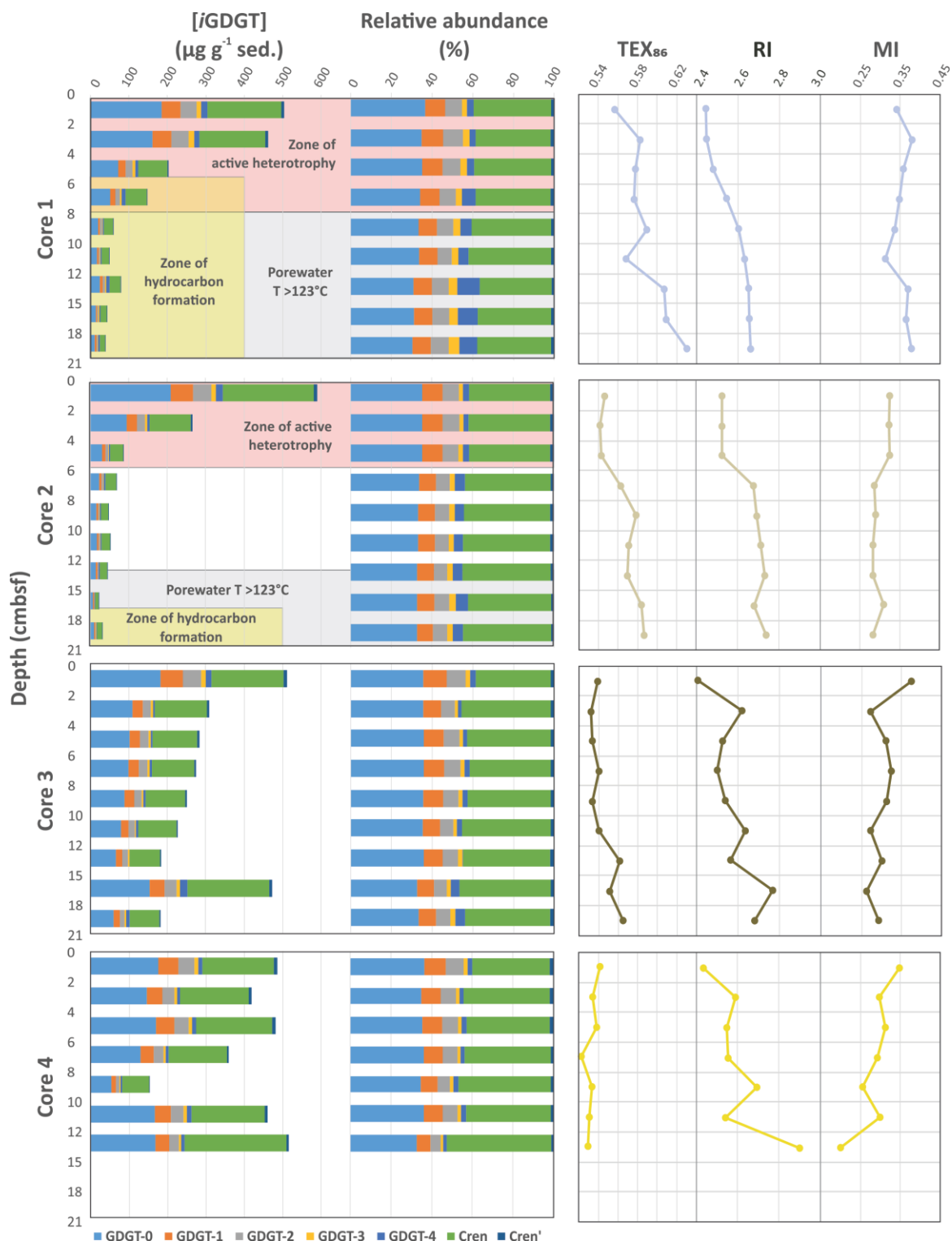
in which C_t and C_i are concentration at time (t) and the initial concentration, respectively (e.g. Schouten et al., 2010). Rearranging Eq. 1, the k' were calculated as

$$k' = (-\ln[C_t / C_i]) / t \quad (2)$$

From these data, it is evident that the down core concentrations of each lipid decrease at equivalent rates (i.e. they have the same slopes for their rates of decay $s^2 = 0.2$). the exception to this is core 2, which independent of two outliers has different decay paths for GDGT-3 and GDGT-5. This is consistent with the TEX₈₆ *i*GDGT lipid classes largely being removed from the sediment lipid pool in a non-selective manner.

Based on these results, the TEX₈₆, ring index (RI), and methane index (MI) values were plotted against their respective summed *i*GDGTs lipid concentrations (Fig 3B–D). For samples located within the habitable zone (having porewaters ranging from 0–123 °C; Kashefi and Lovley, 2003), no correlation is observed between the lipid abundances and proxy ratios of TEX₈₆, RI, or MI (Figure 3B–D). This further suggests these proxies are not affected by turnover in the habitable zone. However, once sediment burial reaches beyond the habitable zone, TEX₈₆ ratios trend to higher values (similarly also reflected in GDGT-3 concentration trends of Figure 3A). Collectively, these data strongly indicate that archaeal lipid turnover is largely nonselective of the TEX₈₆ lipid classes and will therefore theoretically not in and of themselves significantly impact archaeal lipid paleoclimate proxy reconstructions.

Apart from paleoclimate reconstructions, archaeal lipid CLs are sometimes used to resolve aspects of localized biogeochemical cycles within sediments. To this end, the location and degree of anaerobic oxidation of methane (AOM) is determined by methane and archaeal lipid carbon isotope measures (e.g. Boetius et al., 2000; Schouten et al., 2003; Stadnitskaia et al., 2008; Biddle et al., 2012) as well as by the proportional abundances of core GDGTs (*c*GDGTs) in the form of the MI (Zhang et al., 2011; Carr et al., 2018; Petrick et al., 2019). With respect to the latter, the MI proxy is used to differentiate regions of normal marine (with values between 0–0.3) and active AOM conditions in and around cold seeps (where values >0.5–1 are reported for gas hydrate impacted sediments and subsurface environments with high AOM levels). To our knowledge, the use of this proxy for hydrothermal vent systems has not been thoroughly investigated even though this microbial process has been well documented at Guaymas Basin. For example, highly ¹³C-depleted CLs reaching up to -70‰ in hydrothermal vent sediments with porewater temperatures as high as 95 °C indicates thermophilic archaea actively engaging in AOM (Schouten et al., 2003). Biddle et al. (2012) through the detection of relevant archaeal communities by 16S RNA in conjunction with highly depleted methane carbon isotope values determined active AOM spanning 35 to 90 °C porewater conditions. AOM is not likely to be the dominant form of carbon and sulfur metabolism as it generally accounts for less than 5% of sulfate reduction (Kallmeyer and Boetius, 2004). When applying the MI to the Cathedral Hill push core transect survey low values (ranging from 0.2–0.38; Table 1) are recorded with no correspondence to thermal controls across the vent transect (Figure 4). Although, it could be considered that the low values arise from a lack of AOM within these sediments the low MI values are consistent with a high upper water column *i*GDGTs loading as estimated by Bentley et al. (2022).



375
 376
 377 **FIGURE 2.** Down core profiles of the Cathedral Hill core *i*GDGTs absolute and relative lipid abundances
 378 and their generated *i*GDGT proxies: TEX₈₆, RI, and MI. The pink background indicates transect intervals
 379 within zones of active GDGT lipid heterotrophy (Bentley et al., 2022). The gray background are transect
 380 regions where porewater temperatures exceeded 123 °C, marking the known upper thermal limit of life
 381 (Kashefi and Lovley, 2003). Yellow fields are zones where oil generation and hydrocarbon degradation occur
 382 (Dalzell et al., 2021).

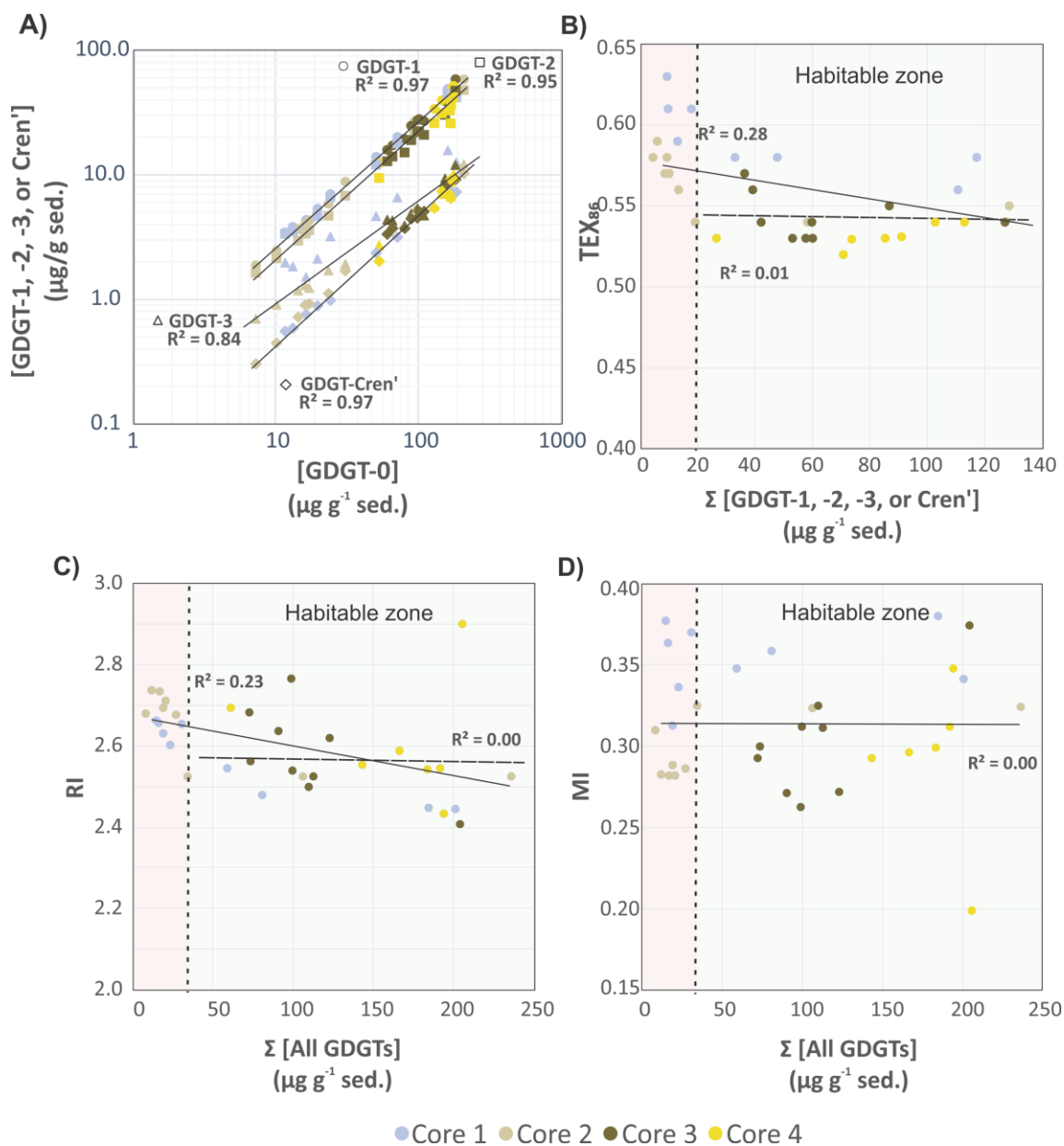


FIGURE 3. A) Comparison of TEX₈₆ lipid concentrations GDGT-1 (circles), -2 (squares), -3 (triangles), and Cren' (diamonds) relative to the GDGT-0. Comparison of B) TEX₈₆, C) RI, and D) MI proxy values relative to summed *i*GDGTs abundances of the Cathedral Hill transect cores. Light green and pink regions indicate areas within and outside the habitable zone of life. Solid and dashed regression lines mark the total number of samples investigated for this study ($n=34$) and those that only reside within the habitable zone where up to 94% of the archaeal lipid turnover occurs ($n=22$), respectively.

3.2. TEX₈₆ and reconstructed SSTs

McClymont et al. (2012) reported a GDGT-based reconstructed annual SSTs of 16–18 °C from particulate organic matter collected in ambient sediment traps in the Guaymas Basin during an annual cycle from 1996–1997. The reconstructed temperatures followed the calibration model for sediments outside of polar regions

proposed by Kim et al. (2010). These authors demonstrated the temperatures derived from the TEX₈₆ reconstruction were significantly lower than those produced by the closely co-varying U₃₇^{k'} paleoclimate proxy, and satellite measured estimates that jointly estimated a mean annual sea surface temperature (MASST) of 23 °C. The longer 21-year (1982–2004) satellite-derived MASST is also reported to be higher at 24 °C (Herrera-Cervantes et al., 2007). Although, the sites and time frames of these surveys do not match that of the Cathedral Hill survey, they do provide context to what our reconstructed TEX₈₆ values should record.

The high sedimentation rate at Cathedral Hill has resulted in near homogenous inputs of organic matter from the upper water column across the transect area (Dalzell et al., 2021; Bentley et al., 2022). Therefore, TEX₈₆ reconstructions should produce equivalent cross-transect trends with sediment depth. Nonetheless, as with changes in the archaeal lipid concentrations, the profiles of *i*GDGT proxies TEX₈₆ and RI of the transect similarly have down core trends (Figure 2; Bentley et al., 2022). For core 4, TEX₈₆ span a narrow range of values (n=7; 0.52–0.54, avg. 0.53 ± 0.01; Figure 4A) across a period of ~37.5 to 75 yrs. corresponding to the depth of the cores. To a slightly lesser degree, the core top (0–2 cmbsf) across the transect also display near-equal values to core 4 (n=4; 0.56–0.54; avg. 0.55 ± 0.01). These values mark a TEX₈₆^H reconstructed mean annual SST of 19.3–20.4 °C following the Kim et al. (2010) calibration model (Table 1). However, the TEX₈₆ values recorded in cores 1 to 3 at Cathedral Hill have considerably larger ranges with values spanning from 0.53 to 0.63 (Table 1) that systematically increase with rising porewater temperatures (R² = 0.83; Table 1; Figure 2 and 4A). This increase is most noticeable in core 1 where the highest TEX₈₆ values are obtained from the bottom core sediments (10–21 cmbsf; marking the non-habitable zone) where TEX₈₆ values span 0.57–0.63 (Table 1; Fig 4A) corresponding to a TEX₈₆^H reconstructed SST change of 3.1 °C marking a range from 21.8 to 24.9 °C (Table 1). The fundamental driver for the proxy's is likely influenced by the archaeal community composition that is responding to their exposure to *in situ* vent fluid temperatures (Figure 4).

Two mechanisms are considered for the observed proxy variations. The first is that progressive ring-loss due to carbon-carbon bond cleavage of pentacyclic rings moieties by exposure to the sharp geothermal gradient acts to systematically attenuate the *i*GDGT lipid pool. Hydrous pyrolysis experiments conducted by Schouten et al. (2004) demonstrated that at extreme temperatures (ca. >160 °C), TEX₈₆ values become negatively impacted by the preferential destruction of polycyclic GDGTs. Such losses produce progressively lower ratio values. Although, the transect sediment porewaters do not reach the pyrolytic temperatures of the Schouten et al. (2004) experiment, they are high enough to generate hydrocarbons (Dalzell et al., 2021) and thermochemically degrade *i*GDGTs in the hottest regions of the transect they are also more long-lived than what is produced from a laboratory experiment. However, the observed stratigraphic TEX₈₆ trends do not match those of predicted ring loss as the values increase rather than decrease in relation to elevated porewater condition. Nonetheless, the thermochemical oxidative loss of GDGTs and its effect on the TEX₈₆ ratio is further explored below (section 3.4).

The second mechanism is that subsurface microbial communities donate enough core GDGTs to overprint the detrital signal source. The RI (Figure 4B) values were similarly compared to recorded porewater temperatures to better interpret the TEX₈₆ trends and to ensure that the Cathedral Hill reconstructed temperatures are influenced by the subsurface microbial community. In this regard, RI is used to monitor the adaptive response of an archaeal community at the hydrothermal vent site. Lipid cyclization is an adaptive response to changing environmental temperature or acidity in which an archaeon increases its rigidity by decreasing the fluidity and permeability of its cellular membrane that, therefore, also further regulates the flow of solutes and nutrients in and out of the cell (Gliozzi et al., 1983; De Rosa and Gambacorta, 1988; Uda et al., 2001; Schouten et al., 2002; Macalady et al., 2004; Boyd et al., 2013). Both cores 1 and 2 have RI values highly correlated to temperature (R² = 0.87 and 0.75, respectively) consistent with heat stress adaption. This same was also observed in the Guaymas Basin by Schouten et al. (2003) who reported an increase in the RI of core lipid GDGTs with *in situ* temperature. As such, a significant proportion of the measured *i*GDGTs likely emanates from archaeal communities living in the shallow sediments of Cathedral Hill. As such, the lipid cyclization pattern may reflect stratigraphically discrete thermophilic to hyperthermophilic communities that are selectively adapted to more extreme temperature conditions (see Bentley et al., 2022 for further discussion on the lipid-based taxonomic make-up of the vent site).

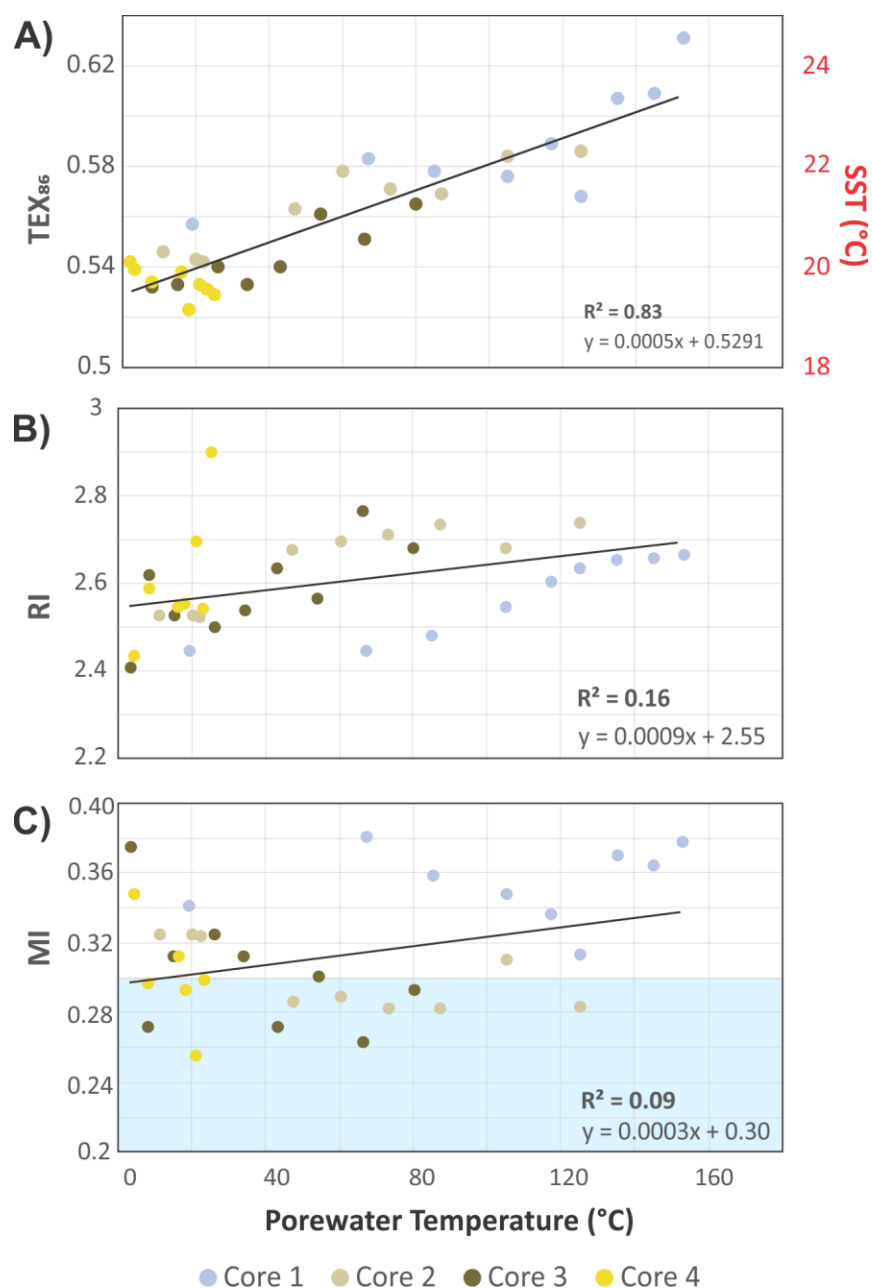


FIGURE 4. Cross plots of A) TEX₈₆, B) RI, and C) MI, *i*GDGT proxies versus porewater temperature. TEX₈₆^Hreconstructed MASSTs are based on Kim et al. (2010). Blue field indicates MI values for normal marine conditions (Zang et al., 2011).

3.3. Lipid signal sourcing

To evaluate the sources of measured archaeal lipids, CL and IPLTEX₈₆ (the ratio applied to IPLs that contain equivalent core lipids) indices were compared as signal responses from their respective pools of living and dead cellular debris (Figure 5). For cores 1, 2, and 3 the 1G-*i*GDGT IPLTEX₈₆ measures are positively correlated with temperature ($R^2 = 0.46, 0.74, \text{ and } 0.66$, respectively; Figure 5A). In this regard, 1G-*i*GDGT

460 $_{IPL}TEX_{86}$ ratio appears to be largely influenced by *in situ* porewater temperatures as well as may by the
 461 archaeal community ecology of the vent system. Factors such as community composition and adaptation
 462 may further impact the $_{IPL}TEX_{86}$ ratio as the rates of changes between cores 1–3 are not the same. Similar to
 463 the $_{CL}TEX_{86}$ values, the $_{IPL}TEX_{86}$ is not correlated to their summed TEX_{86} lipid abundances (Figure 5B). Such
 464 a condition is largely consistent with the living lipid pool being modified by the archaeal community's
 465 response to thermal stress and not by subsequent thermal-oxidative transformation occurring shortly after cell
 466 death.
 467 The IPL and CL lipids of transect samples can be further grouped into three clusters (A, B, C), suggesting a
 468 mixed signal for the sourcing of archaeal GDGTs from both the living and dead pools of archaea (Figure 5C)
 469 closely tracking temperature. In this plot, we assume that clusters falling on the 1:1 line indicate the living
 470 biota can equally contribute to the dead pool of total recovered GDGTs. Those off-axis contribute either less
 471 or more to one or the other lipid pool. The three clusters mark unique thermal zones within the transect area
 472 with cluster A being composed of the ambient core 2 to 4 seafloor surface samples; cluster B marking a mix
 473 of intermediate temperature samples from all cores; and cluster C being composed of high temperatures
 474 samples. The lipid groups likely mark distinct archaeal communities. As cluster B resides on the 1:1 line, the
 475 TEX_{86} core lipids likely have a mix of detrital and *in situ* inputs. Cluster C, however, appears likely dominated
 476 by *in situ* lipid production. The thermal zonation and equivalent directionality of the resulting ratios (i.e., both
 477 CL and $_{IPL}TEX_{86}$ ratios increase with porewater temperature) further supports overprinting of the original
 478 $_{CL}TEX_{86}$ sea surface signal by the ocean bottom sediment archaeal community as a mechanism for the
 479 observed $_{CL}TEX_{86}$ trends.
 480
 481 Collectively, these results suggest the source of the archaeal CLs measured in the TEX_{86} and RI indices
 482 progressively become more dominated by subsurface microbial communities adapted to the hotter
 483 hydrothermal vent fluids. Our results also indicate that in select natural environments, such as hydrothermal
 484 vent complexes, the TEX_{86} SST-proxy may entirely record ocean bottom sediment porewater temperatures.
 485 To our knowledge, a clear case of overprinting to this level has not yet been demonstrated.
 486

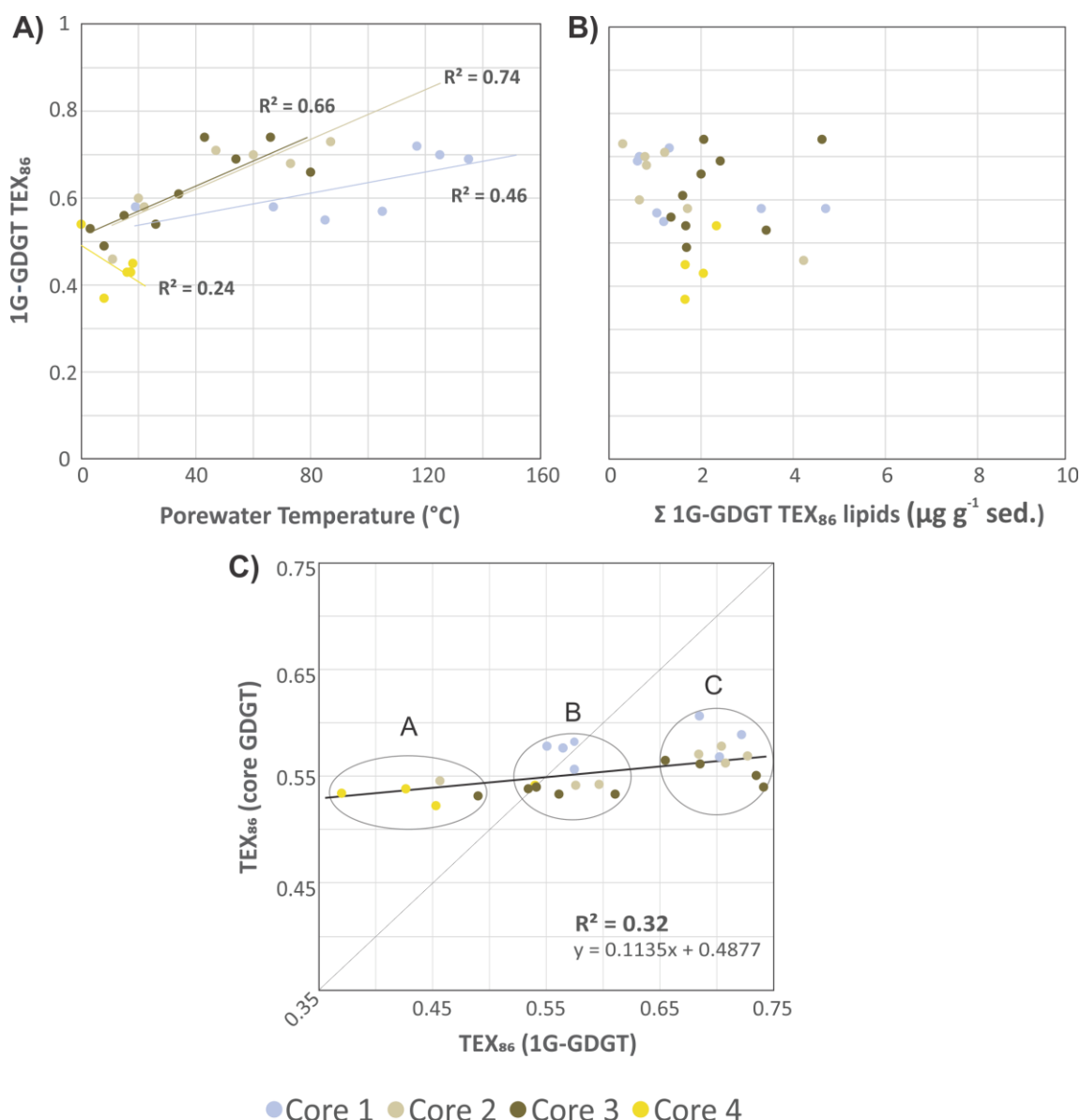


FIGURE 5. Cross plots of 1G-*i*GDGTs $_{IPL}TEX_{86}$ versus (A) porewater temperatures and (B) the concentration of 1G-*i*GDGTs in the sediments. C) TEX_{86} proxy of core GDGTs vs 1G-GDGTs. Clusters A–C may represent different archaeal communities that are providing varying inputs of *i*GDGT to the core GDGT lipid pool. The dotted trendline is the partial least square regression of the complete core lipid TEX_{86} data set. The solid line marks the 1:1 CL to IPL proxy correspondence indicating both allochthonous and autochthonous sources contribute equally to the core GDGT lipid pool.

3.4. TEX_{86} overprint corrections

The measured TEX_{86} ($_{M}TEX_{86}$) value of the Cathedral Hill sediments is herein considered to be a weighted sum of a sea surface TEX_{86} ($_{SS}TEX_{86}$) value acquired from lipids sourced in the upper water column that is further modified by a component of the deeper water column sourced core lipids ($_{WC}TEX_{86}$) as well as by additions of archaeal lipids from the benthic and subsurface microbial communities ($_{Sed}TEX_{86}$). These ratio

loadings are collectively also potentially further modified by diagenetic influences in the ocean bottom sediments. Over the cumulative sediment burial period and in consideration of the measured porewater temperatures of the Cathedral Hill push core sediments, these influences include the selective loss of lipids by their binding into protokerogen (K) and by potential changes due to the loss of lipid by turnover (ϕ ; section 3.1). Additional catagenetic effects from thermochemical alteration of lipids (θ) may also attenuate the sum of sedimentary core lipids by their exposure to high temperature vent fluids. Collectively, these effects are considered to form the following relationship:

$${}_M\text{TEX}_{86} = \frac{a_{ss}\text{TEX}_{86} + b_{wc}\text{TEX}_{86} + c(d_{0-n})_{Sed}\text{TEX}_{86}}{\phi + K + \theta} \quad (3)$$

where a , b , and c , are measured scaling parameters for lipid loading and ϕ , K , and θ are diagenetic and catagenetic alteration parameters. Solving for $ss\text{TEX}_{86}$:

$$ss\text{TEX}_{86} = \frac{{}_M\text{TEX}_{86}(\phi + K + \theta)}{a} - \frac{b_{wc}\text{TEX}_{86} + c(d_{0-n})_{Sed}\text{TEX}_{86}}{a} \quad (4)$$

In this regard, a portion of the archaeal community from the upper water column, presumably initially sourced of IPLs, and an additional community inhabiting the ocean floor sediments were assumed to eventually die with their respective IPLs gradually hydrolyze, joining the CL pool where they further contribute to the observed ${}_M\text{TEX}_{86}$ value. For this study, no data was collected to calculate $b_{wc}\text{TEX}_{86}$ and its potential impact on ${}_M\text{TEX}_{86}$ cannot be further considered in this study. However, it is highly likely, given the longer residence times for glycosidic-based headgroups of the identified archaeal IPLs and their relatively short settling time through the water column (Lengger et al., 2012; Xie et al., 2013) that a component of this lipid source was already mixed with the $sed\text{TEX}_{86}$ contribution. For this study, $sed\text{TEX}_{86}$ is an $IPL\text{TEX}_{86}$ ratio based on detected 1G-GDGT-1, -2, -3, Cren' and 2G-GDGT-1, -2, as present in the original paleoclimate proxy (Table 1; Figure 6). Testing the removal of 2G-GDGTs lipids, which have a low absolute concentration ($<2 \mu\text{g g}^{-1} \text{ sed.}$) and shallow stratigraphic zones of occurrence (section 3.1; Table S2), yielded a negligible $<1^\circ\text{C}$ change in the summed average reconstructed SST.

The $c(d_{0-n})$ measured scaling parameter was calculated as

$$c(d_{0-n}) = \sum_{i=0}^n \left(\frac{[\text{GDGTs}_{IPL-\text{TEX}_{86} \text{ lipids}}]_n}{[\text{GDGTs}_{CL-\text{TEX}_{86} \text{ lipids}}]_{0-2cm}} \right) \quad (5)$$

using the summed concentrations of 1G- and 2G-GDGTs that have the potential to become converted to $c\text{GDGTs}$ by progressive burial diagenesis and d_{0-n} marking the range of sampled sediment depths, with 0 being the 0-2cmbsf core top and n the deepest point of sediment burial. These intervals are divided by the water column input of TEX_{86} lipids ($[\text{GDGTs}_{CL-\text{TEX}_{86} \text{ lipids}}]_{0-2cm}$) estimated to be $120 \mu\text{g g}^{-1} \text{ sed.}$ based on their average measured concentration across the four-core transect. The function assumes the surface sediment does not hydrolyze its IPL-GDGTs to CLs (Table 2). When applied to Eq. 4 and further excluding ϕ , K , and θ , the $ss+wc\text{TEX}_{86}^H$ reconstructed SSTs average $19.68 \pm 0.79^\circ\text{C}$ (Table 2; Figure 6A) with the total samples having an unchanging depth profile that mirrors the range of values measured in the ambient sediments of core 4 (Figure 2).

The selective lipid removal by diagenetic and catagenetic processes theoretically may also affect the TEX_{86} value; however, their perspective impact on the directionality and magnitude of the ratio are difficult to predict and equally hard to discretely measure. Although the loss of GDGTs to protokerogen formation could potentially impact the ratio, it was shown to be a negligible sink for the lipids (Bentley et al., 2022). As such, the K parameter in Eqs. 3 and 4 was therefore assigned a 0 value. Due to the high geothermal gradient at Cathedral Hill, some of the transect push core sediments resided within zones of active catagenesis (Fig. 2; Dalzell et al., 2021). The degradation rates of each TEX_{86} lipid were independently measured for the four push cores (Eq. 2; Fig. S2). As the abundance of both CLs and IPLs differentially decreases through the various core sediment profiles with turnover rates that appear to be constrained by porewater temperature

changes (section 3.1), the degradation rates must also record the effects of thermochemical oxidative weathering (Fig. 3B). In this case, ϕ and θ are treated as grouped parameters. To determine if individual lipid classes were selectively removed during degradation, the variance (s^2) of the rate change as measured from its respective regression slope (i.e. $m_{\log k'}$) from the TEX₈₆ lipids (Figure S2; Table S4 from Eq. 2) were calculated. For the Cathedral Hill transect, the calculated $m_{\log k'}$ s^2 is 0.20, which is due to accelerated degradation rates for higher ring lipids, GDGT-3 and Cren', in samples from cores 1 and 2, where high vent temperatures resulted in hydrocarbon generation of the sediments (Dalzell et al., 2021). A weighing function for the degree of lipid class selectivity during turnover is proposed:

$$\phi + \theta = 1 / {}_M\text{TEX}_{86}^{0.2} \quad (6)$$

When applied to Eq. 4, the corrected data series produces an average transect ${}_{SS+WC}\text{TEX}_{86}^H$ reconstructed SST of 23.66 ± 0.59 °C with a near-zero partial least squares regression slope (Table 2; Figure 6B). As these modeled values are within the 23–24 °C obtained for the 21-year (1982–2004) satellite-derived MASST data for the Guaymas Basin region (Herrera-Cervantes et al., 2007). Based on these calculations, nearly all ${}_M\text{TEX}_{86}$ attenuation can be attributed to sediment microbial overprinting coupled to diagenetic and catagenetic loss of lipids consistent with prior observations at Guaymas Basin (Schouten et al., 2003; Zhang et al., 2011). The high degree of influence this has on the TEX₈₆ proxy is striking given that the upper water flux of GDGTs at Cathedral Hill is estimated to represents up to 93% of the total intact polar and core GDGT lipid pool within these sediments. Although, this study demonstrates the benthic microbial community can influence TEX₈₆ values in anomalous, end-member environments; the above model has not yet been tested across conventional ocean shelf environments.

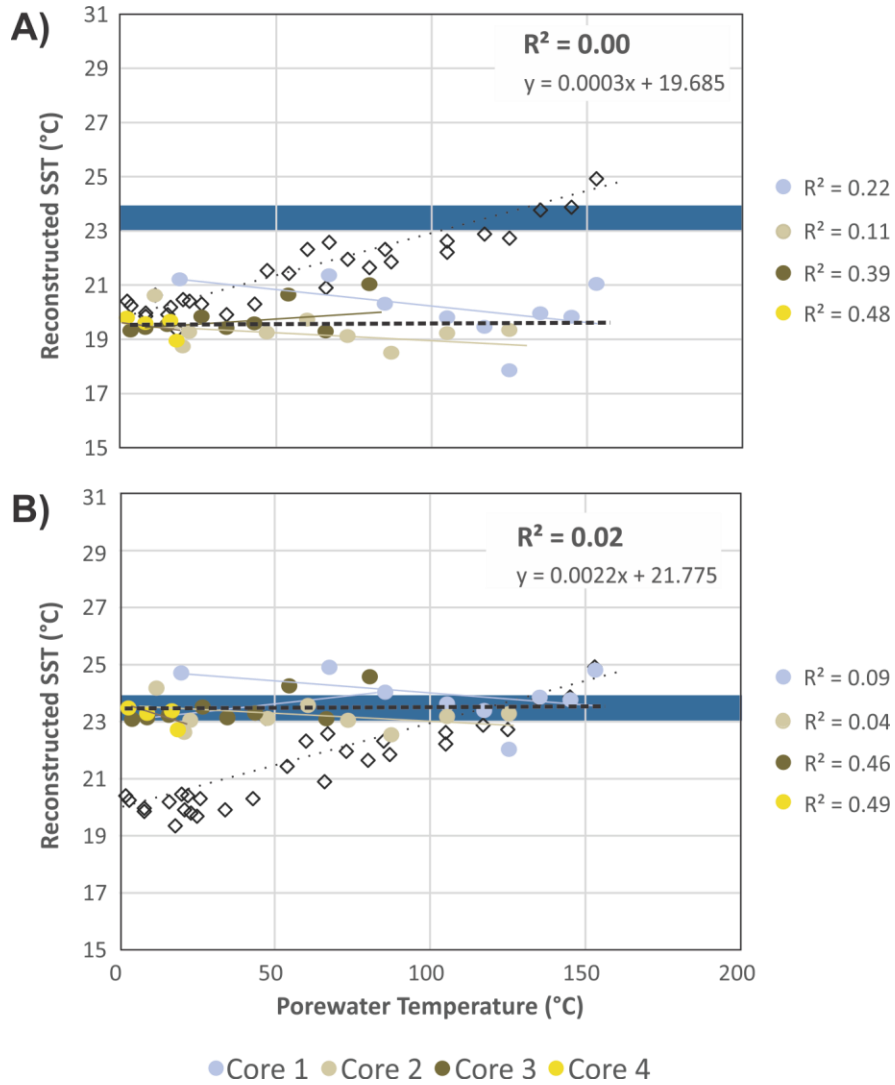


FIGURE 6. Reconstructed combined $_{SS}TEX_{86}$ and SSTs $_{WC}TEX_{86}$ from Eq. 4 (A) with and (B) without ϕ , K , and θ scaling parameters compared to measured porewater temperatures. Colored circles indicate recorded values from the four push cores. $_{M}TEX_{86}$ values are plotted for reference (open black diamonds). Blue field is the 23–24 °C range observed for the 21-year (1982–2004) satellite-derived MASST data (Herrera-Cervantes et al., 2007).

579 **Table 2.** Reconstructed sea surface temperatures.
580

Sample	Depth (cmbsf)	Porewater Temp. (°C)	<i>t</i> Time (yrs.)	^M TEX ₈₆ (Measured iGDGT TEX ₈₆)	TEX ₈₆ ^H Reconstructed SST (°C)	TEX ₈₆ 1G- & 2G- GDGT IPLs (µg g ⁻¹)	Cumulative 1G- & 2G- GDGTs Loading with Depth (µg g ⁻¹)	^{Sed} TEX ₈₆ (i.e. 1G- & 2G-GDGT IPL TEX ₈₆)	<i>c</i> (<i>d</i> _{0-n}) Cumulative Weighted IPL Loading (Eq. 5)
Core 1 (0-2cm)	1	19	10	0.56	21.2	4.80	0	0.58	0.00
Core 1 (2-4cm)	3	67	20	0.58	22.6	3.41	4.80	0.58	0.04
Core 1 (4-6cm)	5	85	30	0.58	22.3	1.29	8.21	0.55	0.07
Core 1 (6-8cm)	7	105	40	0.58	22.2	1.14	9.50	0.57	0.08
Core 1 (8-10cm)	9	117	50	0.59	22.9	1.41	10.64	0.72	0.09
Core 1 (10-12cm)	11	125	60	0.57	21.8	0.76	12.05	0.70	0.10
Core 1 (12-15cm)	13	135	70	0.61	23.8	0.72	12.81	0.69	0.11
Core 1 (15-18cm)	17	145	80	0.61	23.9	0.00	13.53	0.69*	0.11*
Core 1 (18-21cm)	20	153	90	0.63	24.9	0.00	13.53	0.69*	0.11*
Avg.				0.59	22.84				
Std. Dev.				0.02	1.16				
Core 2 (0-2cm)	1	11	10	0.55	20.6	4.33	0	0.49	0.00
Core 2 (2-4cm)	3	22	20	0.54	20.4	1.80	4.33	0.57	0.04
Core 2 (4-6cm)	5	20	30	0.54	20.5	0.76	6.13	0.60	0.05
Core 2 (6-8cm)	7	47	40	0.56	21.5	1.31	6.89	0.73	0.06
Core 2 (8-10cm)	9	60	50	0.58	22.3	0.88	8.20	0.70	0.07
Core 2 (10-12cm)	11	73	60	0.57	22.0	0.92	9.08	0.68	0.08
Core 2 (12-15cm)	13	87	70	0.57	21.8	0.40	10.00	0.73	0.08
Core 2 (15-18cm)	17	105	80	0.58	22.6	0.00	10.40	0.73*	0.09
Core 2 (18-21cm)	20	125	90	0.59	22.7	0.00	10.40	0.73*	0.09*
Avg.				0.56	21.61				
Std. Dev.				0.02	0.91				
Core 3 (0-2cm)	1	3.2	10	0.54	20.2	3.51	0	0.56	0.03
Core 3 (2-4cm)	3	8	20	0.53	19.9	1.79	3.51	0.51	0.01
Core 3 (4-6cm)	5	15	30	0.53	19.9	1.45	5.30	0.57	0.01
Core 3 (6-8cm)	7	26	40	0.54	20.3	1.77	6.74	0.55	0.01
Core 3 (8-10cm)	9	34	50	0.53	19.9	1.70	8.51	0.61	0.01
Core 3 (10-12cm)	11	43	60	0.54	20.3	2.16	10.21	0.71	0.02
Core 3 (12-15cm)	13	54	70	0.56	21.4	2.52	12.37	0.69	0.02
Core 3 (15-18cm)	17	66	80	0.55	20.9	4.72	14.89	0.73	0.04
Core 3 (18-21cm)	20	80	90	0.57	21.6	2.10	19.61	0.65	0.02
Avg.				0.54	20.50				
Std. Dev.				0.01	0.67				
Core 4 (0-2cm)	1	2	10	0.54	20.4	2.43	0	0.54	0.02
Core 4 (2-4cm)	3	8	20	0.53	20.0	1.75	2.43	0.44	0.01
Core 4 (4-6cm)	5	16	30	0.54	20.2	2.15	4.18	0.49	0.02

Core 4 (6-8cm)	7	18	40	0.52	19.3	1.76	6.34	0.47	0.01
Core 4 (8-10cm)	9	21	50	0.53	19.9	0.44	8.09	-	-
Core 4 (10-12cm)	11	23	60	0.53	19.8	2.20	8.54	-	-
Core 4 (12-15cm)	13	25	70	0.53	19.7	0.00	10.74	-	-
Avg.				0.53	19.90				
Std. Dev.				0.01	0.34				
Cumulative Avg.					19.68				
Cumulative Std. Dev.					0.79				

* Marks inherited values from the above sediment horizon.

Table 2. Reconstructed sea surface temperatures (continued).

Sample	Eq. 4 excluding $\phi+\theta+K$			Eq. 4 including $\phi+\theta+K$		
	$SS+WC\overline{TEX}_{86} (M\overline{TEX}_{86} - c(d_{0-n}) * \overline{Sed} \overline{TEX}_{86})$	$SS+WC\overline{TEX}_{86}^H$ (after Kim et al., 2010)	$SS+WC\overline{TEX}_{86}^H$ Reconstructed SST ($^{\circ}C$)	$\phi+\theta$ (Eq. 6) (where $s^2 = 0.20$; Table S4)	$SS+WC\overline{TEX}_{86}$	$SS+WC\overline{TEX}_{86}^H$ Reconstructed SST ($^{\circ}C$) (after Kim et al., 2010)
Core 1 (0-2cm)	0.56	-0.25	21.2	1.12	0.63	24.7
Core 1 (2-4cm)	0.56	-0.25	21.4	1.12	0.63	24.9
Core 1 (4-6cm)	0.54	-0.27	20.3	1.13	0.62	24.2
Core 1 (6-8cm)	0.53	-0.27	19.8	1.13	0.61	23.9
Core 1 (8-10cm)	0.52	-0.28	19.5	1.14	0.61	23.7
Core 1 (10-12cm)	0.50	-0.30	17.9	1.15	0.58	22.6
Core 1 (12-15cm)	0.53	-0.27	20.0	1.13	0.62	24.2
Core 1 (15-18cm)	0.53	-0.27	19.8	1.13	0.61	24.1
Core 1 (18-21cm)	0.55	-0.26	21.0	1.13	0.63	25.0
Avg.	0.54	-0.27	20.10	1.13	0.61	24.14
Std. Dev.	0.02	0.02	1.08	0.01	0.02	0.75
Core 2 (0-2cm)	0.55	-0.26	20.6	1.13	0.62	24.2
Core 2 (2-4cm)	0.52	-0.28	19.2	1.14	0.60	23.3
Core 2 (4-6cm)	0.51	-0.29	18.7	1.14	0.59	22.9
Core 2 (6-8cm)	0.52	-0.28	19.3	1.14	0.60	23.4
Core 2 (8-10cm)	0.53	-0.28	19.7	1.14	0.61	23.8
Core 2 (10-12cm)	0.52	-0.28	19.1	1.14	0.60	23.4
Core 2 (12-15cm)	0.51	-0.29	18.5	1.14	0.59	23.0
Core 2 (15-18cm)	0.52	-0.28	19.2	1.14	0.60	23.5
Core 2 (18-21cm)	0.52	-0.28	19.3	1.14	0.60	23.6
Avg.	0.52	-0.28	19.32	1.14	0.60	23.47
Std. Dev.	0.01	0.01	0.60	0.00	0.01	0.40
Core 3 (0-2cm)	0.52	-0.28	19.4	1.14	0.60	23.3
Core 3 (2-4cm)	0.52	-0.28	19.4	1.14	0.60	23.3
Core 3 (4-6cm)	0.53	-0.28	19.5	1.14	0.60	23.4
Core 3 (6-8cm)	0.53	-0.27	19.9	1.13	0.60	23.6
Core 3 (8-10cm)	0.52	-0.28	19.4	1.14	0.60	23.3
Core 3 (10-12cm)	0.53	-0.28	19.6	1.14	0.60	23.5
Core 3 (12-15cm)	0.55	-0.26	20.7	1.13	0.62	24.3
Core 3 (15-18cm)	0.52	-0.28	19.3	1.14	0.60	23.4
Core3 (18-21cm)	0.55	-0.26	21.0	1.13	0.62	24.6
Avg.	0.53	-0.27	19.79	1.14	0.60	23.64
Std. Dev.	0.01	0.01	0.62	0.00	0.01	0.49
Core 4 (0-2cm)	0.53	-0.27	19.8	1.13	0.60	23.6
Core 4 (2-4cm)	0.53	-0.28	19.7	1.14	0.60	23.4

Core 4 (4-6cm)	0.53	-0.28	19.8	1.14	0.60	23.5
Core 4 (6-8cm)	0.52	-0.29	19.0	1.14	0.59	22.9
Core 4 (8-10cm)	-	-	-	-	-	-
Core 4 (10-12cm)	-	-	-	-	-	-
Core 4 (12-15cm)	-	-	-	-	-	-
Avg.	0.53	-0.28	19.51	1.07	0.60	23.38
Std. Dev.	0.01	0.01	0.38	0.00	0.01	0.31
Cumulative Avg.			19.68			23.66
Cumulative Std. Dev.			0.79			0.59

581
582
583

584 4. Conclusions

585 In this study, we demonstrate a pronounce overprint of *c*GDGTs sourced from the ocean floor sedimentary
586 archaeal community at the Cathedral Hill vent site in Guaymas Basin. The overprint is marked by lipids with
587 more cyclized ring moieties marking an adaptive response by archaea to rigidify the cellular membranes
588 against localized heat stress. This in turn has resulted in the commonly used TEX₈₆ paleoclimate proxy to
589 partially record advecting porewaters temperatures. As the vast majority of *c*GDGTs in these sediments is
590 sourced from the overlying water column, the impact on the TEX₈₆ ratio is further the product of rapid lipid
591 turnover rates and diagenetic and catagenetic alteration processes potentially unique to the hydrothermal
592 system. Together, these factors resulted in absolute TEX₈₆^H temperature offsets of up to 4 °C based on
593 calibrations closely suited to the latitudinal position of Guaymas Basin. To untangle the impact of these
594 coupled drivers on the TEX₈₆ proxy, we further present a method to correct the overprints by both the water
595 column and subsurface archaeal community using IPLs extracted from both of these sources. Although, we
596 have not been able to test this model with lipid inputs from the overlying water column, we have demonstrated
597 its effectiveness at removing sediment sourced overprints, which may not be unique to hydrothermal systems.
598 This approach should be capable of being extended to all near-surface marine sediment systems and may
599 improve the quality of calibration models or climate reconstructions that are based on modern TEX₈₆
600 measures.

601
602
603
604

604 Acknowledgments

605 A special thank you is extended to Associate Editor Jack Middelburg and the reviewers of Biogeosciences
606 who provided highly constructive feedback. We are grateful to Carl Peters, formally at Saint Mary's
607 University, who contributed considerable feedback and advice during the course of this study. We further
608 thank the officers, crew, and pilots of the R/V Atlantis and HOV Alvin for their expert help at sea and their
609 outstanding efforts acquiring the samples for this study. Julius Lipp, Florence Schubotz, and Kai-Uwe
610 Hinrichs of MARUM, assisted our lab in the development of lipidomic analytical techniques. Special thanks
611 is extended to Clarissa Sit for the use of her HPLC-qToFMS. Sean Sylvia assisted with the preparation of
612 push cores used in sampling. Funding for this study is through NSERC Canadian Research Chair, Canada
613 Foundation for Innovation (CFI) JELF-CRC, NSERC Discovery Grant (Application Number: RGPIN-2017-
614 05822), WHOI Deep Ocean Exploration Initiative 2008, and NSF grant MCB-0702677 (to JSS and SMS).

615
616
617
618

617 Conflicts of Interest

618 The authors declare no conflict of interest.

619
620

620 Supplementary information

621 Supplementary material related to this article can be found on-line at <https://doi.org/.....>

622

623 References

- 624 Bentley, J. N., Ventura, G. T., Dalzell, C. J., Walters, C. C., Peters, C. A., Mennito, A. S., Nelson, R. K.,
625 Reddy, C. M., Walters, C. J., Seewald, J., & Sievert, S. M. (2022). Archaeal lipid diversity, alteration,
626 preservation at Cathedral Hill, Guaymas Basin, and its link to the deep time preservation paradox.
627 Organic Geochemistry. 163:104302. doi.org/10.1016/j.orggeochem.2021.104302.
628
- 629 Besseling, M., Hopmans, E. C., Koenen, M., van der Meer, M. T. J., Vreugdenhil, S., Schouten, S.,
630 Sinninghe Damsté, J. S., & Villanueva, L. (2019). Depth-related differences in archaeal populations
631 impact the isoprenoid tetraether lipid composition of the Mediterranean Sea water column. Organic
632 Geochemistry, 135, 16–31. doi.org/10.1016/j.orggeochem.2019.06.008.
- 633 Besseling, M. A., Hopmans, E. C., Bale, N. J., Schouten, S., Sinninghe Damsté, J. S., & Villanueva, L.
634 (2020). The absence of intact polar lipid-derived GDGTs in marine waters dominated by Marine
635 Group II: Implications for lipid biosynthesis in Archaea. Sci Rep 10, 294. doi.org/10.1038/s41598-
636 019-57035-0.
637
- 638 Biddle, J. F., Cardman, Z., Mendlovitz, H., Albert, D. B., Lloyd, K. G., Boetius, A., & Teske, A. (2012).
639 Anaerobic oxidation of methane at different temperature regimes in Guaymas Basin hydrothermal
640 sediments. The ISME Journal 6, 1018–1031. doi.org/10.1038/ismej.2011.164.
641
- 642 Boetius, A., Ravensschlag, K., Schubert, C., Rickert, D., Widdel, F., Gieseke, A., Amann, R., Jørgensen,
643 B.B, Witte, U., & Pfannkuche, O. (2000). A marine microbial consortium apparently mediating
644 anaerobic oxidation of methane. Nature 407, 623–626. <https://doi.org/10.1038/35036572>.
645
- 646 Boyd, E., Hamilton, T., Wang, J., He, L., & Zhang, C. (2013). The role of tetraether lipid composition in
647 the adaptation of thermophilic archaea to acidity. Frontiers in Microbiology, 4, 62.
648
- 649 Brochier- Armanet, C., Boussau, B., Gribaldo, S., & Forterre, P. (2008). Mesophilic Crenarchaeota:
650 proposal for a third archaeal phylum, the Thaumarchaeota. National Review Microbiology 6, 245–
651 252. doi:10.1038/nrmicro1852.
652
- 653 Carr, S. A., Schubotz, F., Dunbar, R. B., Mills, C. T., Dias, R., Summons, R. E., & Mandernack, K. W.
654 (2018). Acetoclastic Methanosaeta are dominant methanogens in organic-rich Antarctic marine
655 sediments. The ISME Journal, 12(2), 330–342. <https://doi.org/10.1038/ismej.2017.150>.
656
- 657 Curray, J. R., Moore, D. G., Lawver, L. A., Emmel, F. J., Raitt, R. W., Henry, M., & Kieckhefer, R. (1979).
658 Tectonics of the Andaman Sea and Burma: convergent margins. In J.S. Watkins, L. Montadert, P.W.
659 Dickerson (Eds.) Geological and Geophysical Investigations of Continental Margins, AAPG Memoir
660 29, 189–198.
661
- 662 Dalzell, C. J., Ventura, G. T., Nelson, R. K., Reddy, C. M., Walters, C. J., Seewald, J., & Sievert, S. M.
663 (2021). Resolution of multi-molecular hydrocarbon transformation in petroleum-bearing sediments
664 from the Cathedral Hill hydrothermal vent complex at Guaymas Basin, Gulf of California by
665 comprehensive two-dimensional gas chromatography and chemometric analyses. Organic
666 Geochemistry, 152, 104173.
667
- 668 De Rosa, M., & Gambacorta, A. (1988). The lipids of archaeobacteria. Progress in lipid research, 27, 153–
669 175.
670
- 671 Elling, F.J., Könneke, M., Lipp, J.S., Becker, K.W., Gagen, E.J., & Hinrichs, K.-U. (2014). Effects of
672 growth phase on the membrane lipid composition of the thaumarchaeon *Nitrosopumilus maritimus*

and their implications for archaeal lipid distributions in the marine environment. *Geochimica et Cosmochimica Acta*, 141, 579–597.

Elling, F. J., Könneke, M., Mußmann, M., Greve, A., & Hinrichs, K. U. (2015). Influence of temperature, pH, and salinity on membrane lipid composition and TEX₈₆ of marine planktonic thaumarchaeal isolates. *Geochimica et Cosmochimica Acta*, 171, 238–255.

Gieskes, J. M., Simoneit, B. R., Brown, T., Shaw, T. J., Wang, Y. C., & Magenheimer, A. (1988). Hydrothermal fluids and petroleum in surface sediments of Guaymas Basin, Gulf of California: a case study. *The Canadian Mineralogist*, 26, 589–602.

Gliozzi, A., Paoli, G., De Rosa, M., & Gambacorta, A. (1983). Effect of isoprenoid cyclization on the transition temperature of lipids in thermophilic archaeobacteria. *Biochimica et Biophysica Acta (BBA)-Biomembranes*, 735, 234–242.

Herrera-Cervantes, H.; Lluch-Cota, D. B., Lluch-Cota, S. E., & Gutiérrez-de-Velasco, S. G. (2007). The ENSO signature in sea-surface temperature in the Gulf of California. *Journal of Marine Research*, 65, 589–605. doi.org/10.1357/002224007783649529.

Herfort, L., Schouten, S., Boon, J. P. & Sinninghe Damsté, J. S. (2006). Application of the TEX₈₆ temperature proxy to the southern North Sea. *Organic Geochemistry* 37, 1715–26.

Ho, S. L. & Laepple, T. (2016). Flat meridional temperature gradient in the early Eocene in the subsurface rather than surface ocean. *Nature Geoscience*, 9, 606–610.

Hollis, C.J., Taylor, K.W.R., Handley, L., Pancost, R.D., Huber, M., Creech, J.B., Hines, B.R., Crouch, E.M., Morgans, H.E.G., Crampton, J.S., Gibbs, S., Pearson, P.N., & Zachos, J.C. (2012). Early Paleogene temperature history of the Southwest Pacific Ocean: Reconciling proxies and models. *Earth and Planetary Science Letters* 349–350, 53–66

Hopmans, E. C., Weijers, J. W., Schefuß, E., Herfort, L., Sinninghe Damsté, J. S., & Schouten, S. (2004). A novel proxy for terrestrial organic matter in sediments based on branched and isoprenoid tetraether lipids. *Earth and Planetary Science Letters*, 224, 107–116.

Huguet, C., Cartes, J. E., Sinninghe Damsté, J. S., & Schouten, S. (2006). Marine crenarchaeotal membrane lipids in decapods: Implications for the TEX₈₆ paleothermometer. *Geochemistry, Geophysics, Geosystems*, 7. doi 10.1029/2006GC001305.

Huguet, C., Martrat, B., Grimalt, J. O., Sinninghe Damsté, J. S. & Schouten, S. (2011). Coherent millennial-scale patterns in U37 k0 and TEX₈₆ H temperature records during the penultimate interglacial-to-glacial cycle in the western Mediterranean. *Paleoceanography* 26. DOI: 10.1029/2010PA002048.

Huguet, C., Schimmelmann, A., Thunell, R., Lourens, L. J., Sinninghe Damsté, J. S., & Schouten, S. (2007). A study of the TEX₈₆ paleothermometer in the water column and sediments of the Santa Barbara Basin, California. *Paleoceanography*, 22. doi 10.1029/2006PA001310.

Hurley, S.J., Elling, F.J., Könneke, M., Buchwald, C., Wankel, S.D., Santoro, A.E., Lipp, J.S., Hinrichs, K.-U., Pearson, A. (2016). Influence of ammonia oxidation rate on thaumarchaeal lipid composition and the TEX₈₆ temperature proxy. *Proceedings of the National Academy of Sciences, U. S. A.* 113, 7762–7767.

Kallmeyer, J., & Boetius, A. (2004). Effects of temperature and pressure on sulfate reduction and anaerobic oxidation of methane in hydrothermal sediments of Guaymas Basin. *Applied and Environmental Microbiology*. 70, 1231–1233. doi.org/10.1128/AEM.70.2.1231-1233.2004.

728 Karner, M. B., DeLong, E. F., Karl, D. M. (2001). Archaeal dominance in the mesopelagic zone of the
729 Pacific Ocean. *Nature*, 25, 409(6819), 507–510. doi: 10.1038/35054051.

730
731 Kashefi, K., & Lovley, D. R. (2003). Extending the upper temperature limit for life. *Science*, 301, 934–934.
732

733 Kim, J. H., Schouten, S., Hopmans, E. C., Donner, B., & Damsté, J. S. S. (2008). Global sediment core-top
734 calibration of the TEX₈₆ paleothermometer in the ocean. *Geochimica et Cosmochimica Acta*, 72,
735 1154–1173.
736

737 Kim, J. H., Van der Meer, J., Schouten, S., Helmke, P., Willmott, V., Sangiorgi, F., Koç, N., Hopmans, E.
738 C. & Damsté, J. S. S. (2010). New indices and calibrations derived from the distribution of
739 crenarchaeal isoprenoid tetraether lipids: Implications for past sea surface temperature
740 reconstructions. *Geochimica et Cosmochimica Acta*, 74, 4639–4654.
741

742 Kim J.-H., Romero O. E., Lohmann G., Donner B., Laepple T., Haam E. & Sinninghe Damsté J. S. (2012a)
743 Pronounced subsurface cooling of North Atlantic waters off Northwest Africa during Dansgaard-
744 Oeschger interstadials. *Earth and Planetary Science Letters*, 339–340, 95–102.
745

746 Kim, J. H., Crosta, X., Willmott, V., Renssen, H., Bonnin, J., Helmke, P., Schouten, S. & Sinninghe
747 Damsté, J. S. (2012b). Holocene subsurface temperature variability in the eastern Antarctic
748 continental margin. *Geophysical Research Letters*, 39. doi 10.1029/2012GL051157.
749

750 Kim J.-H., Schouten, S., Rodrigo-Gamiz, M., Rampen, S., Marino, G., Huguet, C., Helmke, P., Buscail, R.,
751 Hopmans, E. C., Pross, J., Sangiorgi, F., Middelburg, J. B. M., & Sinninghe Damsté J. S. (2015).
752 Influence of deep-water derived isoprenoid tetraether lipids on the paleothermometer in the
753 Mediterranean Sea. *Geochimica et Cosmochimica Acta*, 150, 125–141.
754

755 Knappy, C. S., Chong, J. P., & Keely, B. J. (2009). Rapid discrimination of archaeal tetraether lipid cores
756 by liquid chromatography-tandem mass spectrometry. *Journal of the American Society for Mass*
757 *Spectrometry*, 20, 51–59.
758

759 Lawrence, K. T., Pearson, A., Castaneda, I. S., Ladlow, C., Peterson, L. C., Lawrence, G. E. (2020).
760 Comparison of Late Neogene U^k₃₇ and TEX₈₆ Paleotemperature records from the eastern equatorial
761 Pacific at orbital resolution. *Paleoceanography and Paleoclimatology*, 35, 1–16.
762

763 Lengger, S.K., Hopmans, E.C., Reichart, G.-J., Nierop, K.G.J., Sinninghe Damsté, J.S., Schouten, S.
764 (2012). Intact polar and core glycerol dibiphytanyl glycerol tetraether lipids in the Arabian Sea
765 oxygen minimum zone. Part II: Selective preservation and degradation in sediments and consequences
766 for the TEX₈₆. *Geochimica et Cosmochimica Acta* 98, 244–258.
767

768 Lengger, S, K, Hopmans, E. C., Sinninghe Damsté, J. S., Schouten, S. (2014). Fossilization and degradation
769 of archaeal intact polar tetraether lipids in deeply buried marine sediments (Peru Margin). *Geobiology*,
770 12(3), 212–220, <https://doi.org/10.1111/gbi.12081>.
771

772 Lipp, J. S., & Hinrichs, K. U. (2009). Structural diversity and fate of intact polar lipids in marine
773 sediments. *Geochimica et Cosmochimica Acta*, 73, 6816–6833.
774

775 Lipp, J. S., Morono, Y., Inagaki, F., & Hinrichs, K. U. (2008). Significant contribution of Archaea to extant
776 biomass in marine subsurface sediments. *Nature*, 454, 991–994.
777

778 Liu, X. L., Leider, A., Gillespie, A., Gröger, J., Versteegh, G. J., & Hinrichs, K. U. (2010). Identification of
779 polar lipid precursors of the ubiquitous branched GDGT orphan lipids in a peat bog in Northern
780 Germany. *Organic Geochemistry*, 41, 653–660.
781

782 Liu, X. -L., Lipp, J. S., Hinrichs, K. -U. (2011). Distribution of core and intact GDGTs in marine sediments.
783 *Organic Geochemistry* 42, 368–375.

784
785 Liu, X. L., Russell, D. A., Bonfio, C., Summons, R. E. (2018) Glycerol configurations of environmental
786 GDGTs investigated using a selective sn2 ether cleavage protocol. *Organic Geochemistry*, 128, 57–
787 62.
788
789 Lopes dos Santos R. A., Prange M., Castaneda I. S., Schefuß E., Mulitza S., Schulz M., Niedermeyer E.
790 M., Sinninghe Damsté J. S. and Schouten S. (2010). Glacial–interglacial variability in Atlantic
791 meridional overturning circulation and thermocline adjustments in the tropical North Atlantic. *Earth*
792 *and Planetary Science Letters*, 300, 407–414.
793
794 Lunt, D. J., Haywood, A. M., Schmidt, G. A., Salzmann, U., Valdes, P. J., Dowsett, H. J., & Loptson, C.A.
795 (2012). On the causes of mid-Pliocene warmth and polar amplification. *Earth and Planetary Science*
796 *Letters*, 321–322, 128–138, doi:10.1016/j.epsl.2011.12.042.
797
798
799 Macalady, J. L., Vestling, M. M., Baumler, D., Boekelheide, N., Kaspar, C. W., & Banfield, J. F. (2004).
800 Tetraether-linked membrane monolayers in *Ferroplasma* spp: a key to survival in
801 acid. *Extremophiles*, 8, 411–419.
802
803 McClymont, E. L., Ganeshram, R. S., Pichevin, L. E., Talbot, H. M., van Dongen, B. E., Thunell, R. C.,
804 Haywood, A.M., Singarayer, J.S. & Valdes, P. J. (2012). Sea-surface temperature records of
805 Termination 1 in the Gulf of California: Challenges for seasonal and interannual analogues of tropical
806 Pacific climate change. *Paleoceanography*, 27. doi 10.1029/2011PA002226.
807
808 McKay, L. J., MacGregor, B. J., Biddle, J. F., Albert, D. B., Mendlovitz, H. P., Hoer, D. R., Lipp, J.S.,
809 Lloyd, K.G & Teske, A. P. (2012). Spatial heterogeneity and underlying geochemistry of
810 phylogenetically diverse orange and white Beggiatoa mats in Guaymas Basin hydrothermal
811 sediments. *Deep Sea Research Part I: Oceanographic Research Papers*, 67, 21–31.
812
813 Meyer, S., Wegener, G., Lloyd, K. G., Teske, A., Boetius, A., & Ramette, A. (2013). Microbial habitat
814 connectivity across spatial scales and hydrothermal temperature gradients at Guaymas
815 Basin. *Frontiers in Microbiology*, 4, 207.
816
817 Naafs, B. D. A., Rohrssen, M., Inglis, G. N., Lähteenoja, O., Feakins, S. J., Collinson, M. E., Kennedy,
818 E.M., Singh, P.K., Singh, M.P., Lunt, D.J., & Pancost, R. D. (2018). High temperatures in the
819 terrestrial mid-latitudes during the early Palaeogene. *Nature Geoscience*, 11, 766–771.
820
821 O'Brien, C.L., Robinson, S.A. Pancost, R.D., Sinninghe Damste, J.S., Schouten, S., Lunt, D.J., Alsenz, H.,
822 Bomemann, A., Bottini, C., Brassell, S.C., Farnsworth, A., Forster, A., Huber, B.T., Inglis, G.N.,
823 Jenkyns, H.C., Linnert, C., Littler, K., Markwick, P., McAnena, A., Mutterlose, J., Naafs, B.D.A.,
824 Puttmann, W., Sluijs, A., van Helmond, N.A.G.M., Vellekoop, J., Wagner, T., & Wrobel, N.E.
825 (2017). Cretaceous sea-surface temperature evolution: Constraints from TEX86 and planktonic
826 foraminiferal oxygen isotopes. *Earth-Science Reviews*. 172, 224–247.
827
828 Pearson, A. & Ingalls, A. E. (2013) Assessing the use of archaeal lipids as marine environmental proxies.
829 *Annual Review Earth Planetary Science*. 41, 15.1–15.26.
830
831 Pearson, A., Huang, Z., Ingalls, A. E., Romanek, C. S., Wiegel, J., Freeman, K. H., Smittenberg, R. H. &
832 Zhang, C. L. (2004). Nonmarine crenarchaeol in Nevada hot springs. *Applied and Environmental*
833 *Microbiology*, 70, 5229–5237.
834
835 Petrick, B., Reuning, L., & Martinez-Garcia (2019) Distribution of Glycerol Dialkyl Glycerol Tetraethers
836 (GDGTs) in Microbial Mats From Holocene and Miocene Sabkha Sediments. *Frontiers in Earth*
837 *Science*. 04. doi.org/10.3389/feart.2019.00310.
838
839

840 Qin, W., Carlson, L. T., Armbrust, E. V., Devol, A. H., Moffett, J. W., Stahl, D. A., & Ingalls, A. E. (2015).
841 Confounding effects of oxygen and temperature on the TEX₈₆ signature of marine Thaumarchaeota.
842 Proceedings of the National Academy of Sciences, U. S. A. 112(35), 10,979–10,984.
843 doi.org/10.1073/pnas.1501568112.
844

845 Robinson, S. A., Ruhl, M., Astley, D. L., Naafs, B. D. A., Farnsworth, A. J., Bown, P. R., Jenkyns, H. C.,
846 Lunt, D. J., O'Brien, C., Pancost, R. D., & Markwick, P. J. (2017). Early Jurassic North Atlantic sea-
847 surface temperatures from TEX₈₆. *Palaeothermometry. Sedimentology*, 64, 215–230.
848

849 Rommerskirchen, F., Condon, T., Mollenhauer, G., Dupont, L. M., & Schefuß, E. (2011). Miocene to
850 Pliocene development of surface and subsurface temperatures in the Benguela Current system.
851 *Paleoceanography*, 26, PA3216, 1-15. doi.org/10.1029/2010PA002074.
852

853 Schouten, S., Hopmans, E. C., & Sinninghe Damsté, J. S. (2013). The organic geochemistry of glycerol
854 dialkyl glycerol tetraether lipids: A review. *Organic Geochemistry*, 54, 19–61.
855

856 Schouten, S., Hopmans, E. C., & Sinninghe Damsté, J. S. (2004). The effect of maturity and depositional
857 redox conditions on archaeal tetraether lipid palaeothermometry. *Organic Geochemistry*, 35, 567–571.
858

859 Schouten, S., Hopmans, E. C., Schefuß, E., & Sinninghe Damsté, J. S. (2002). Distributional variations in
860 marine crenarchaeotal membrane lipids: a new tool for reconstructing ancient sea water
861 temperatures? *Earth and Planetary Science Letters*, 204, 265–274.
862

863 Schouten S., Wakeham S. G., Hopmans E. C. and Sinninghe Damsté J. S. (2003) Biogeochemical Evidence
864 that Thermophilic Archaea Mediate the Anaerobic Oxidation of Methane. *Appl. Environ. Microbiol.*
865 69, 1680-1686.
866

867 Seki, O., Bendle, J. A., Haranda, N., Kobayashi, M., Sawada, K., Moossen, H., Inglis, G. N., Nagao, S., &
868 Sakamoto, T. (2014). Assessment and calibration of TEX₈₆ paleothermometry in the Sea of Okhotsk
869 and sub-polar North Pacific region: Implications for paleoceanography. *Progress in Oceanography*.
870 126, 254–266.
871

872 Sinninghe Damsté J. S., Rijpstra W. I. C., Hopmans E. C., den Uijl M. J., Weijers J. W. H. and Schouten S.
873 (2018) The enigmatic structure of the crenarchaeol isomer. *Organic Geochemistry* 124, 22-28.
874

875 Stadnitskaia, A., Nadezhkin, D., Abbas, B., Blinova, V., Ivanov, M. K., & Sinninghe Damsté, J. S. (2008).
876 Carbonate formation by anaerobic oxidation of methane: evidence from lipid biomarker and fossil
877 16S rDNA. *Geochimica et Cosmochimica Acta*, 72(7), 1824–1836.
878

879 Sturt, H. F., Summons, R. E., Smith, K., Elvert, M., & Hinrichs, K. U. (2004). Intact polar membrane lipids
880 in prokaryotes and sediments deciphered by high-performance liquid chromatography/electrospray
881 ionization multistage mass spectrometry—new biomarkers for biogeochemistry and microbial
882 ecology. *Rapid communications in mass spectrometry*, 18, 617–628.
883

884 Teske, A., Callaghan, A. V., & LaRowe, D. E. (2014). Biosphere frontiers of subsurface life in the
885 sedimented hydrothermal system of Guaymas Basin. *Frontiers in Microbiology*, 5, 362.
886

887 Teske, A., De Beer, D., McKay, L. J., Tivey, M. K., Biddle, J. F., Hoer, D., Lloyd, K.G., Lever, M.A., Røy,
888 H., Albert, D.B & MacGregor, B. J. (2016). The Guaymas Basin hiking guide to hydrothermal
889 mounds, chimneys, and microbial mats: Complex seafloor expressions of subsurface hydrothermal
890 circulation. *Frontiers in Microbiology*, 7, 75.
891

892 Tierney, J. E. (2014). Biomarker-based inferences of past climate: the TEX₈₆ paleotemperature proxy. In
893 H.D. Holland & K.K. Turekian (Eds.) *Treatise on Geochemistry* (2nd Ed.) 12, 379-939.
894

895 Uda, I., Sugai, A., Itoh, Y. H., & Itoh, T. (2001). Variation in molecular species of polar lipids from
896 *Thermoplasma acidophilum* depends on growth temperature. *Lipids*, 36, 103–105.
897

898 Umoh, U., Li L., Luckge, A., Schwartz-Schampera, U., & Naafs, D. (2020). Influence of hydrothermal vent
899 activity on GDGT pool in marine sediments might be less than previously thought. *Organic*
900 *Geochemistry*. 104102. doi.org/10.1016/j.orggeochem.2020.104102.
901

902 Wakeham, S. G., Lewis, C. M., Hopmans, E. C., Schouten, S., & Sinninghe Damsté, J. S. (2003). Archaea
903 mediate anaerobic oxidation of methane in deep euxinic waters of the Black Sea. *Geochimica et*
904 *Cosmochimica Acta*, 67, 1359–1374.
905

906 Weijers, J. W., Schefuß, E., Kim, J. H., Sinninghe Damsté, J. S., & Schouten, S. (2014). Constraints on the
907 sources of branched tetraether membrane lipids in distal marine sediments. *Organic Geochemistry*, 72,
908 14–22.
909

910 Weijers, J. W., Schouten, S., van den Donker, J. C., Hopmans, E. C., & Sinninghe Damsté, J. S. (2007).
911 Environmental controls on bacterial tetraether membrane lipid distribution in soils. *Geochimica et*
912 *Cosmochimica Acta*, 71, 703–713.
913

914 Wuchter, C., Schouten, S., Wakeham, S. G., & Sinninghe Damsté, J. S. (2005). Temporal and spatial
915 variation in tetraether membrane lipids of marine Crenarchaeota in particulate organic matter:
916 Implications for TEX₈₆ paleothermometry. *Paleoceanography*, 20, doi 10.1029/2004PA001110.
917

918 Wuchter, C., Schouten, S., Wakeham, S. G. & Sinninghe Damsté, J. S. (2006). Archaeal tetraether
919 membrane lipid fluxes in the northeastern Pacific and the Arabian Sea: implications for TEX₈₆
920 paleothermometry. *Paleoceanography* 21.
921

922 Xie, S., Lipp, J.S., Wegener, G., Ferdelman, T.G., Hinrichs, K-U. (2013). Turnover of microbial lipids in
923 the deep biosphere and growth of benthic archaeal populations. *Proceedings of the National Academy*
924 *of Sciences, U. S. A.* 110, 6010–6014.
925

926 Yoshinaga, M. Y., Kellermann, M. Y., Rossel, P. E., Schubotz, F., Lipp, J. S., & Hinrichs, K. U. (2011).
927 Systematic fragmentation patterns of archaeal intact polar lipids by high-performance liquid
928 chromatography/electrospray ionization ion-trap mass spectrometry. *Rapid Communications in Mass*
929 *Spectrometry*, 25, 3563–3574.
930

931 Zeng, Z., Liu, X. L., Farley, K. R., Wei, J. H., Metcalf, W. W., Summons, R. E., & Zhang, Y. G., Pagani,
932 M., & Wang, Z. (2016). Ring Index: A new strategy to evaluate the integrity of TEX₈₆
933 paleothermometry. *Paleoceanography*, 31, 220–232.
934

935 Zhang, Y. G., Zhang, C. L., Liu, X. L., Li, L., Hinrichs, K. U., & Noakes, J. E. (2011). Methane Index: A
936 tetraether archaeal lipid biomarker indicator for detecting the instability of marine gas hydrates. *Earth*
937 *and Planetary Science Letters*, 307, 525–534.
938

939 Zhang, Y. G., Pagani, M. & Wang, Z. (2016). Ring Index: A new strategy to evaluate the integrity of
940 TEX₈₆ paleothermometry. *Paleoceanography and Paleoclimatology* 31:220–232, doi.org/
941 10.1002/2015PA002848.
942

943 Zhu, C., Lipp, J. S., Wörmer, L., Becker, K. W., Schröder, J., & Hinrichs, K. U. (2013). Comprehensive
944 glycerol ether lipid fingerprints through a novel reversed phase liquid chromatography-mass
945 spectrometry protocol. *Organic Geochemistry*, 65, 53–62.